

ssROC: Semi-Supervised ROC Analysis for Reliable and Streamlined Evaluation of Phenotyping Algorithms

Jianhui Gao^{†1}, Clara-Lea Bonzel^{†2}, Chuan Hong³, Paul Varghese⁴, Karim Zakir¹, and Jessica Gronsbell^{1,5,6}

¹*Department of Statistical Sciences, University of Toronto, Toronto, ON, Canada*

²*Department of Biomedical Informatics, Harvard Medical School, Boston, MA, USA*

³*Department of Biostatistics and Bioinformatics, Duke University, Durham, NC, USA*

⁴*Verily Life Sciences, Cambridge, MA, USA*

⁵*Department of Family and Community Medicine, University of Toronto, Toronto, ON, Canada*

⁶*Department of Computer Science, University of Toronto, Toronto, ON, Canada*

Correspondence to:

Jessica Gronsbell

Postal address: 700 University Ave, Toronto, ON, Canada, M5G 1Z5

Email: j.gronsbell@utoronto.ca.

Telephone number: 416-978-3452

Keywords: Electronic Health Records; Phenotyping; Semi-supervised; ROC Analysis

Word count: 3905/4000

ABSTRACT

Objective: High-throughput phenotyping will accelerate the use of electronic health records (EHRs) for translational research. A critical roadblock is the extensive medical supervision required for phenotyping algorithm (PA) estimation and evaluation. To address this challenge, Numerous weakly-supervised learning methods have been proposed. However, there is a paucity of methods for reliably evaluating the predictive performance of PAs when a very small proportion of the data is labeled. To fill this gap, we introduce a semi-supervised approach (ssROC) for estimation of the receiver operating characteristic (ROC) parameters of PAs (e.g., sensitivity, specificity).

Materials and methods: ssROC uses a small labeled dataset to nonparametrically impute missing labels. The imputations are then used for ROC parameter estimation to yield more precise estimates of PA performance relative to classical supervised ROC analysis (supROC) using only labeled data. We evaluated ssROC through in-depth simulation studies and an extensive evaluation of six PAs from Mass General Brigham.

Results: In both simulated and real data, ssROC produced ROC parameter estimates with significantly lower variance than supROC for a fixed amount of labeled data. For the six PAs, the estimates from ssROC are approximately 40% less variable than supROC on average.

Discussion: ssROC enables precise evaluation of PA performance without demanding large volumes of labeled data. ssROC is also easily implementable in open-source R software.

Conclusion: When used in conjunction with weakly-supervised PAs, ssROC facilitates the reliable and streamlined phenotyping necessary for EHR-based research.

BACKGROUND AND SIGNIFICANCE

Electronic Health Records (EHRs) are a vital source of data for clinical and translational research [1]. Vast amounts of patient data are being tapped for real-time studies of infectious diseases, development of clinical decision support tools, and genetic studies at unprecedented scale [2–10]. This myriad of opportunities rests on the ability to accurately and rapidly extract a wide variety of patient phenotypes (e.g., diseases) to both identify and characterize populations of interest. However, precise and readily available phenotype information is rarely available in patient records and presents a major barrier to EHR-based research [11, 12].

In practice, phenotypes are extracted from patient records with either rule-based or machine learning (ML)-based phenotyping algorithms (PAs) derived from codified and natural language processing (NLP)-derived features [13, 14]. While PAs can characterize clinical conditions with high accuracy, they traditionally require a substantial amount of medical supervision that limits the automated power of EHR-based studies [15]. Several research networks have spent considerable effort developing PAs over the last decade, including i2b2 (Informatics for Integrating Biology & the Bedside), the eMERGE (Electronic Medical Records and Genomics) Network, and the OHDSI (Observational Health Data Sciences and Informatics) program that released the APHRODITE (Automated PHenotype Routine for Observational Definition, Identification, Training, and Evaluation) framework [16].

Typically, PA development consists of two key steps: (i) algorithm estimation and (ii) algorithm evaluation. Algorithm estimation determines the appropriate aggregation of

features extracted from patient records to determine phenotype status. For a rule-based approach, medical and informatics experts assemble a comprehensive set of features and corresponding logic to assign patient phenotypes [12, 13]. As this manual assembly can be highly laborious, significant effort has been made to automate the algorithm estimation step with ML. Numerous studies have demonstrated success with PAs derived from standard supervised learning methods such as penalized logistic regression, random forest, and deep neural networks [17–24]. The scalability of a supervised approach, however, is limited by the substantial number of gold-standard labels required for model training. Gold-standard labels, which require time-consuming manual medical chart review, are infeasible to obtain for a large volume of records [25, 26].

In response, semi-supervised and weakly-supervised methods for PA estimation that substantially decrease or eliminate the need for gold-standard labeled data have been proposed. Among semi-supervised methods, self-learning and surrogate-assisted semi-supervised learning are common [27–29]. For example, [15] introduced PheCAP, a common pipeline for semi-supervised learning that utilizes silver-standard labels for feature selection prior to supervised model training to decrease the labeling demand. Unlike gold-standard labels, silver-standard labels can be automatically extracted from patient records (e.g., ICD codes or free-text mentions of the disease) and serve as proxies for the gold-standard label [30, 31]. PheCAP was based on the pioneering work of [32] and [33], which introduced weakly-supervised PAs trained entirely on silver-standard labels. These methods completely eliminate the need for medical chart review for algorithm estimation and are the basis of the APHRODITE framework. Moreover, this work prompted numerous developments in weakly-supervised PAs, including methods based on non-negative matrix/tensor factorization, parametric mixture modeling, and neural network-based em-

bedding learning, which are quickly becoming the new standard in the PA literature [14].

In contrast to the success in automating PA estimation, there has been little focus on the algorithm evaluation step. Algorithm evaluation assesses the predictive performance of a PA, typically through the estimation of the receiver operating characteristic (ROC) parameters such as sensitivity and specificity. At a high-level, the ROC parameters measure how well a PA discriminates between phenotype cases and controls relative to the gold-standard. As phenotypes are the foundation of EHR-based studies, it is critical to reliably evaluate the ROC parameters to provide researchers with a sense of trust in using a PA [34–36]. However, complete PA evaluation is performed far too infrequently due to the burden of chart review [14, 25, 37].

To address this challenge, [38] proposed the first semi-supervised method for ROC parameter estimation. This method assumes that the predictive model is derived from a penalized logistic regression model and was only validated on 2 PAs with relatively large labeled data sets (455 and 500 labels). [25] later introduced PheValuator, and its recent successor PheValuator 2.0, to efficiently evaluate rule-based algorithms using “probabilistic gold-standard” labels generated from diagnostic predictive models rather than chart review [37]. Although the authors provided a comprehensive evaluation for numerous rule-based PAs, PheValuator can lead to biased ROC analysis, and hence a distorted understanding of the performance of a PA, when the diagnostic predictive model is not well-calibrated [39–41]. PheValuator is also only applicable for the evaluation of rule-based PAs.

To fill this gap in the PA literature, we introduce the semi-supervised approach of [38]

to precisely estimate the ROC parameters of PAs, which we call “ssROC”. The key difference between ssROC and classical ROC analysis (supROC) using only labeled data is that ssROC imputes missing gold-standard labels in order to leverage large volumes of unlabeled data (i.e., records without gold-standard labels). By doing so, ssROC yields less variable estimates than supROC to enable reliable PA evaluation with fewer gold-standard labels. Moreover, ssROC imputes the missing labels with a nonparametric calibration of the predictions from the PA to ensure that the resulting estimates of the ROC parameters are unbiased when the PA is not well-calibrated.

OBJECTIVE

The primary objectives of this work are to:

1. Extend the proposal of [38] to a wider class of weakly-supervised PAs that are commonly used in the PA literature, including a theoretical analysis and development of a statistical inference procedure demonstrating good finite-sample properties.
2. Provide an in-depth real data analysis of PAs for six phenotypes from Mass General Brigham (MGB) together with extensive simulation studies to illustrate the practical utility of ssROC.
3. Release an implementation of ssROC in open-source R software to encourage the use of our method by the informatics community.

Through real and simulated data analyses, we observe substantial gains in estimation precision from ssROC relative to supROC. In the analysis of the six PAs from MGB, the estimates from ssROC are approximately 40% less variable than supROC on average. Our results suggest that, when used together with weakly supervised PAs, ssROC can

facilitate the reliable and streamlined PA development that is necessary for EHR-based research.

MATERIALS AND METHODS

Overview of ssROC

We focus on evaluating a classification rule derived from a PA with ROC analysis. ROC analysis assesses the agreement between the gold-standard label for a binary phenotype (e.g., disease case/control), Y , and a PA score, S , indicating a patient’s likelihood of having the underlying phenotype (e.g., the predicted probability of being a disease case). Y is typically obtained from chart review and S can be derived from various phenotyping methods. In this article, we primarily consider PAs derived from weakly-supervised learning methods due to their ability to automate PA estimation and increasing popularity in the informatics literature [14].

In classical supervised ROC analysis, it is assumed that the data is fully labeled and one has information on both Y and S for all subjects. However, in the phenotyping setting, Y is typically only available for a very small subset of patient records due to the laborious nature of medical chart review. This gives rise to the *semi-supervised setting* in which a small labeled dataset is accompanied by a much larger unlabeled dataset. To fully leverage all of the available data and facilitate more reliable (i.e., lower variance) evaluation of PAs, ssROC imputes the missing Y with a nonparametric calibration of S , denoted as $\hat{m}(S)$, to make use of the unlabeled data. A schematic representation of ssROC is provided in Figure 1.

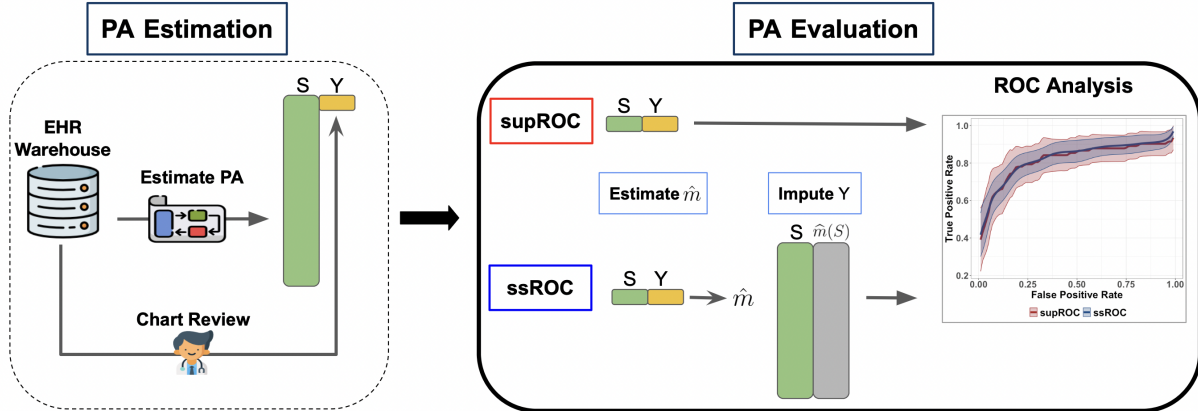


Figure 1: **Overview of PA estimation and evaluation.** The phenotyping algorithm (PA) is first estimated to obtain the scores (S). Patient charts from the electronic health record (EHR) warehouse are reviewed to obtain the gold-standard label (Y) for PA evaluation. In classical supervised ROC analysis (supROC), only the labeled data from chart review is used to evaluate the PA’s performance. Semi-supervised ROC analysis (ssROC), uses the labeled data to impute the missing Y as $\hat{m}(S)$ so that the unlabeled data can be utilized for estimation to yield more precise estimates of the ROC parameters.

Data structure & notation

More concretely, the available data in the semi-supervised setting consists of a small labeled dataset

$$\mathcal{L} = \{(Y_i, S_i) \mid i = 1, \dots, n\}$$

and an independent unlabeled dataset

$$\mathcal{U} = \{S_i \mid i = n + 1, \dots, n + N\}.$$

In the classical semi-supervised setting, it is assumed that (i) \mathcal{U} is a much larger than \mathcal{L} so that $n \ll N$ and (ii) the observations in \mathcal{L} are randomly selected from the underlying pool of data. Throughout our discussion, we suppose that a higher value of S is more indicative of the phenotype. An observation is deemed to have the phenotype if $S > c$,

where c is the threshold used for phenotype classification.

ROC analysis

More formally, ROC analysis evaluates a PA based on the true positive rate (TPR), the false positive rate (FPR), the positive predictive value (PPV), and the negative predictive value (NPV). In the diagnostic testing literature, the TPR is referred to as sensitivity, while the FPR is 1 minus the specificity [42]. For a given classification threshold, one may evaluate the ROC parameters by enumerating the correct and incorrect classifications. This information can be summarized in a confusion matrix as shown in Figure 2.

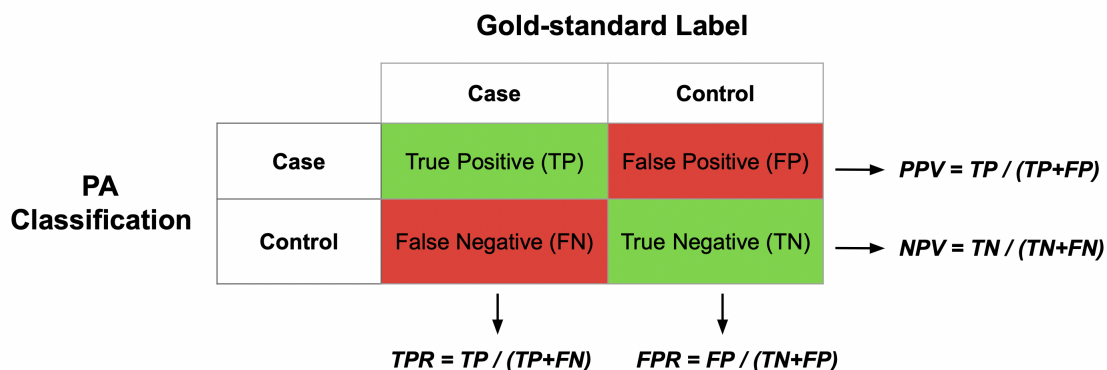


Figure 2: **Confusion matrix.** The algorithm score from the PA is used to determine phenotype case/control status based on the classification threshold. The ROC parameters are evaluated by enumerating the number of correct and incorrect classifications relative to the gold-standard label.

In practice, it is the task of the researcher to estimate an appropriate threshold for classification. This is commonly done by summarizing the trade-off between the TPR and FPR, defined respectively as

$$TPR(c) = P(S > c \mid Y = 1) \text{ and } FPR(c) = P(S > c \mid Y = 0).$$

The ROC curve, $\text{ROC}(u) = \text{TPR}[\text{FPR}^{-1}(u)]$, summarizes the TPR and FPR across all possible choices of the threshold. In the context of PAs, c is often chosen to achieve a low FPR [22]. An overall summary measure of the discriminative power of S in classifying Y is captured by the area under the ROC curve (AUC),

$$\text{AUC} = \int_0^1 \text{ROC}(u) du.$$

The AUC is equivalent to the probability that a phenotype case has a higher value of S than a phenotype control. For a given threshold, the predictive performance of the classification rule derived from the PA is assessed with the PPV and NPV, defined respectively as

$$\text{PPV}(c) = P(Y = 1 \mid S > c), \quad \text{and} \quad \text{NPV}(c) = P(Y = 0 \mid S < c).$$

supROC: classical supervised ROC analysis

With only labeled data, one may obtain supervised estimators of the ROC parameters (supROC) based on their empirical counterparts. For example, the TPR and FPR can be estimated as

$$\widehat{\text{TPR}}_{sup}(c) = \frac{\sum_{i=1}^n Y_i I(S_i > c)}{\sum_{i=1}^n Y_i} \quad \text{and} \quad \widehat{\text{FPR}}_{sup}(c) = \frac{\sum_{i=1}^n (1 - Y_i) I(S_i > c)}{\sum_{i=1}^n (1 - Y_i)}$$

$I(\cdot)$ denotes the indicator function. The PPV and NPV can be estimated analogously. A point along the ROC curve is given by $\widehat{\text{ROC}}_{sup}(u_0) = \widehat{\text{TPR}}_{sup}(\hat{c}_{u_0}) = \widehat{\text{TPR}}_{sup} \left[\widehat{\text{FPR}}_{sup}^{-1}(u_0) \right]$ while the AUC may be obtained from standard numerical integration of the estimated

ROC curve [43]. For a selected threshold, variance estimates are obtained with a resampling-based procedure such as bootstrap or perturbation resampling [44, 45].

ssROC: semi-supervised ROC Analysis

Unlike its supervised counterpart that relies on only the labeled data, ssROC contains two steps of estimation to make use of both the labeled and unlabeled data and provide a more reliable understanding of a PA’s performance. In the first step, the missing labels are imputed with a calibration model trained on the gold standard labels and the PA scores. In the second step, the imputations are used in lieu of the gold-standard labels to evaluate the ROC parameters with the PA scores in the unlabeled data in an analogous manner to supROC. Figure 3 provides a high-level overview of these two steps using the TPR as an example.

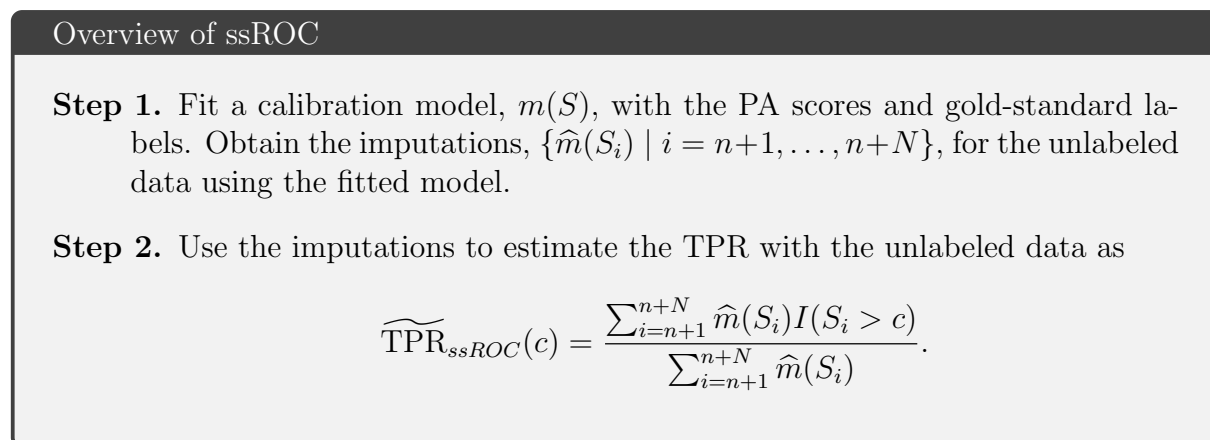


Figure 3: **Two steps of ssROC using the true positive rate (TPR) as an example.**

The purpose of the first step is to ensure that the imputations do not introduce bias into the ROC parameter estimates. For example, utilizing the PA scores directly for imputation can distort the ROC parameter estimates due to potential inaccuracies of S

in predicting Y . We propose to use a kernel regression model to nonparametrically impute the missing labels to prevent biasing the ssROC estimates [40]. Technical detail related to fitting the kernel regression model is provided in Supplementary Section 1. On the other hand, the purpose of the second step is to harness the large unlabeled dataset to produce estimates with lower variance than supROC. Similar to supROC analysis, we propose a perturbation resampling procedure for variance estimation and detail two commonly used confidence intervals (CIs) based on the resampling procedure in Supplementary Section 2. In Supplementary Section 3, we provide a brief theoretical justification for the improved efficiency of ssROC relative to supROC for a wide variety of weakly-supervised PAs.

Data and metrics for evaluation

We assessed the performance of ssROC using both simulated and real-world EHR data from MGB.

Simulation study

We considered two settings representing a PA with high and low accuracy. In both settings, we generated Y from a Bernoulli distribution with a prevalence of 0.3. We generated S from a normal mixture model with a small amount of additive noise as $S | Y = y \sim N(\mu_y, \sigma) + \text{Bin}(1, p_y)$ for $y = 0, 1$. This design was chosen to mimic the use of a weakly supervised PA based on parametric mixture modeling as in our real-world data analysis. The two settings were obtained by varying $(\mu_0, \mu_1, \sigma, p_0, p_1)$ as:

- **Setting 1: PA with low accuracy.** S is generated from the mixture model with $(\mu_0, \mu_1, \sigma, p_0, p_1) = (0, 0.15, 0.25, 0.1, 0.3)$ to yield an AUC of approximately 70.5.

- **Setting 2: PA with high accuracy.** S is generated from the mixture model with $(\mu_0, \mu_1, \sigma, p_0, p_1) = (-0.7, 1, 0.5, 0.3, 0.3)$ to yield an AUC of approximately 96.1.

In both settings, we let the size of the unlabeled data be $N = 10,000$ and varied the labeled size as $n = 100$ and 200 , resulting in a total of 4 simulation studies. We summarize results across 2,000 simulated datasets for each study.

Real-world EHR data application

We validated our method using real-world EHR data from MGB, a Boston-based health-care system anchored by two tertiary care centers, Brigham and Women’s Hospital and Massachusetts General Hospital. We evaluated the PAs for six phenotypes, including Cerebral Aneurysm (CA), Congestive Heart Failure (CHF), Intracranial Hemorrhage (ICH), Parkinson’s Disease (PD), Systemic Sclerosis (SS), and Type 1 Diabetes (T1DM). The data is from the Research Patient Data Registry of MGB which stores data on over 1 billion visits containing diagnoses, medications, procedures, laboratory information, and clinical notes from 1991 to 2017.

The underlying full data for each phenotype consisted of patient records with at least one phenotype-related PheCode in their record [46]. A subset of patients was randomly sampled from the full data and sent for chart review. The average size of the labeled and unlabeled data were 128 and 48,183, respectively. For each phenotype, the PA was obtained by fitting PheNorm without the random corruption denoising step. PheNorm is a recently proposed weakly-supervised method based on normalizing silver-standard labels with respect to patient healthcare utilization using a normal mixture model. PheNorm is described in detail in Supplementary Section 4 [47]. The silver-standard labels were taken as the total numbers of (i) phenotype-related PheCodes and (ii) positive mentions

of the phenotype-related clinical concepts in patient records. Clinical concepts were extracted from clinical notes with the Narrative Information Linear Extraction and mapped to concept unique identifiers (CUIs) in the Unified Medical Language System [48, 49]. The phenotypes represent varying levels of PA accuracy, differences in labeled and unlabeled dataset sizes (n and N , respectively), and prevalence (P). A summary of the six phenotypes is presented in Table 1.

| Phenotype | n | N | P | PheCode | CUI |
|--------------------------------|-----|--------|------|---------|----------|
| Cerebral Aneurysm (CA) | 134 | 18679 | 0.68 | 433.5 | C0917996 |
| Congestive Heart Failure (CHF) | 140 | 155112 | 0.18 | 428 | C0018801 |
| Intracranial Hemorrhage (ICH) | 88 | 47271 | 0.80 | 430 | C0151699 |
| Parkinson’s Disease (PD) | 97 | 17752 | 0.62 | 332 | C0030567 |
| Systemic Sclerosis (SS) | 189 | 4272 | 0.43 | 709.3 | C0036421 |
| Type 1 Diabetes (T1DM) | 121 | 46013 | 0.17 | 250.1 | C0011854 |

Table 1: **Summary of the MGB Phenotypes.** The labeled dataset size (n), the unlabeled dataset size (N), and the prevalence (P) of the six phenotypes as well as the main PheCode and concept unique identifier (CUI) used to train PheNorm. The underlying full data for each phenotype included all participants who passed the filter of ≥ 1 PheCode for the phenotype of interest.

Benchmark method and reported metrics

We compared the PA evaluation results from ssROC and the benchmark, supROC, using the real and simulated data. In the simulation study, we first applied the expit transform to restrict the range of S to $(0,1)$. For both the real and simulated data analyses, we transformed the PA scores by their empirical cumulative distribution function to improve the performance of the kernel regression step [50]. We used the Gaussian kernel with the bandwidth determined by the standard deviation of the standardized PA scores di-

vided by $n^{0.45}$ [38]. We obtained standard error estimates for the ROC parameters using perturbation resampling with 500 replications and weights sampled from a scaled beta distribution given by $4 \cdot \text{Beta}(1/2, 3/2)$ to improve finite-sample performance [51]. We focused on logit-based confidence intervals (CIs) due to their improved performance relative to standard Wald intervals [52]. To obtain the logit-based intervals, we applied a logit transformation to the resampled estimates, computed a Wald-based interval with the transformed estimates, and then converted the upper and lower confidence bounds back to the original scale.

In simulations, the ground truth was the median of the ROC estimates using the completely labeled data across the replicated datasets. We assessed bias for both supROC and ssROC by computing the median of [(point estimate - ground truth)] across the simulated datasets. We also computed the empirical standard error (ESE) as the standard deviation of the estimates across the replicated datasets and the asymptotic standard error (ASE) as the median of the standard error estimates from the perturbation resampling procedure across the replicated datasets. Using mean squared error (MSE) as an aggregate measure of bias and variance, we evaluated the relative efficiency (RE) as the ratio of the MSE of supROC to the MSE of ssROC. The performance of our resampling procedure was assessed with the coverage probability (CP) of the 95% CIs for both estimation procedures. In the real data analysis, we present point estimates from both supROC and ssROC and the RE defined as the ratio of the variance of supROC to ssROC. We evaluated the performance of the PAs at an FPR of 10% and report the results for the AUC, classification threshold (Threshold), TPR, PPV, and NPV for both the real and simulated data.

RESULTS

Simulation Study

We present point estimates and percent biases for the ROC parameters at an FPR of 10% for both simulation settings in Table 2. Both supROC and ssROC showed minimal bias across all ROC parameters, labeled dataset sizes, and simulation settings. The RE of ssROC compared to supROC is illustrated in Figure 4. The median RE for low PA accuracy (setting 1) is 1.1 and 1.6 for the high PA accuracy (setting 2). The higher gain in efficiency highlights the benefits of ssROC relative to supROC, particularly when the PA score is highly informative of the gold-standard label. The most substantial improvements in the RE are observed for PPV when PA accuracy is high and for the Threshold when PA accuracy is low. In setting 1 with $n = 200$, the RE for the PPV is 2.3. Similarly, in setting 1 with $n = 200$, the RE for the Threshold is 2.0. An RE exceeding 1 indicates that ssROC has a smaller variance than supROC (assuming the point estimates from the two procedures are comparable). Alternatively, one may view a reduction in variance in terms of the sample size required for ssROC to achieve the same variance as supROC. Again using PPV as an example, an RE of 2.3 suggests that ssROC with $n = 87$ can achieve the same variance as supROC with $n = 200$.

Supplementary Tables 1 and 2 present the ESE, ASE, and CP of the 95% CIs for simulation settings 1 and 2, respectively. The proposed logit-based CI consistently achieved coverage close to the nominal level for both methods across all settings and parameters. The tables also illustrate the benefit of the logit-based interval over the standard Wald interval, particularly when the ROC parameter estimate is near 0 or 1. For example, in setting 2 with $n=100$, the CPs of the Wald CIs for AUC are 90.6% for supROC and 88.3%

for ssROC) while the CPs of the logit-based intervals are 98.4% and 93.2%, respectively.

| n | Method | AUC | | Threshold | | TPR | | PPV | | NPV | |
|-----------------------------|--------|-------|-------|-----------|-------|-------|-------|-------|-------|-------|-------|
| | | Est. | Bias | Est. | Bias | Est. | Bias | Est. | Bias | Est. | Bias |
| Simulation Setting 1 | | | | | | | | | | | |
| 100 | supROC | 70.76 | -0.11 | 83.35 | -0.14 | 32.43 | 0.71 | 56.30 | -1.30 | 75.68 | 0.22 |
| 100 | ssROC | 70.53 | -0.34 | 83.39 | -0.10 | 32.04 | 0.33 | 56.10 | -1.50 | 75.62 | 0.17 |
| 200 | supROC | 70.75 | -0.14 | 83.40 | -0.09 | 32.11 | 0.37 | 57.03 | -0.57 | 75.54 | 0.06 |
| 200 | ssROC | 70.60 | -0.29 | 83.45 | -0.04 | 31.86 | 0.12 | 56.87 | -0.72 | 75.50 | 0.02 |
| Simulation Setting 2 | | | | | | | | | | | |
| 100 | supROC | 96.13 | -0.02 | 66.98 | 0.22 | 86.99 | -0.56 | 78.46 | -0.48 | 94.22 | -0.19 |
| 100 | ssROC | 95.97 | -0.18 | 66.90 | 0.15 | 86.78 | -0.77 | 78.64 | -0.30 | 94.14 | -0.26 |
| 200 | supROC | 96.18 | 0.03 | 66.74 | 0.00 | 87.57 | 0.01 | 78.76 | -0.21 | 94.44 | 0.03 |
| 200 | ssROC | 96.07 | -0.08 | 66.80 | 0.06 | 87.24 | -0.32 | 78.83 | -0.14 | 94.30 | -0.11 |

Table 2: **Point estimates and percent bias for both simulation settings at a FPR of 10%.** For both settings, the size of the unlabeled was $N = 10,000$.

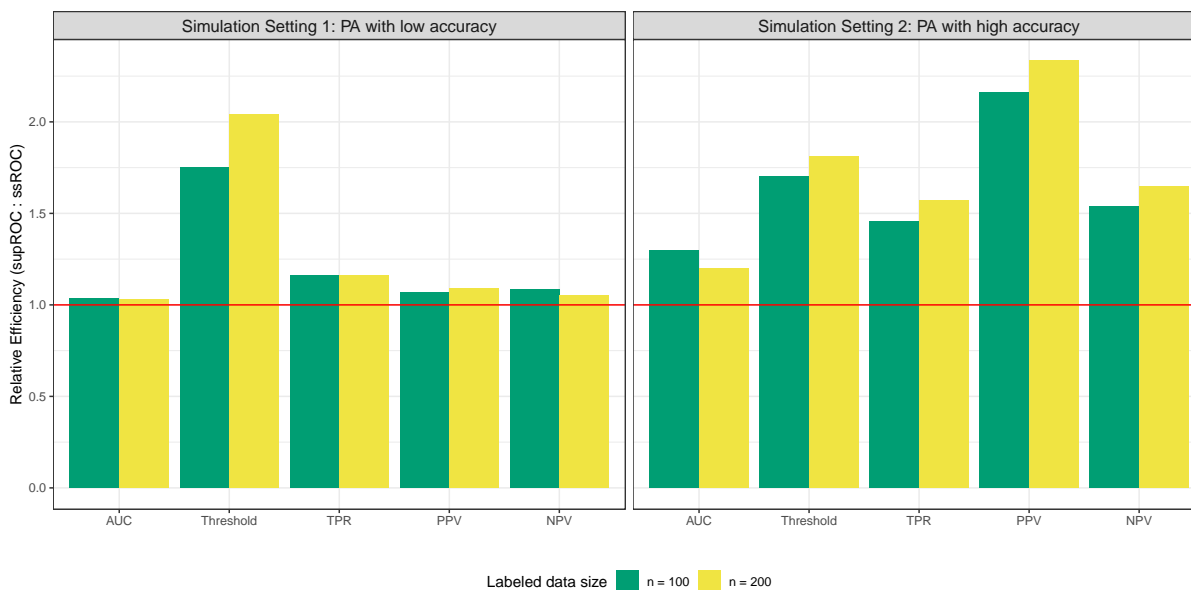


Figure 4: **Relative efficiency for both simulation settings at a FPR of 10%.** Relative efficiency is defined as the mean squared error of supROC compared to the mean squared error of ssROC. For both settings, the size of the unlabeled was $N = 10,000$.

Analysis of six PAs from MGB

Table 3 presents the point estimates for the six phenotypes from MGB, ordered by the AUC estimates from ssROC, at a false positive rate (FPR) of 10%. As our primary focus is to compare ssROC with supROC, a single FPR was chosen for consistency across the phenotypes. However, this does lead to low TPRs for some phenotypes, such as CHF. Generally, the point estimates from ssROC are similar to those from supROC. There are some differences in the classification threshold estimates for CA and SS, which leads to some discrepancies in the corresponding point estimates for the TPR, PPV, and NPV. As supROC is only evaluated at the unique PA scores in the labeled dataset, the Threshold estimate can be unstable at some FPRs. In contrast, ssROC evaluates the ROC parameters across a broader range of PA scores in the larger unlabeled dataset and results in a more stable estimation.

| Phenotype | Method | AUC | Threshold | TPR | PPV | NPV |
|-----------|--------|------|-----------|------|------|------|
| CA | ssROC | 81.3 | 64.0 | 51.0 | 89.8 | 51.5 |
| | supROC | 80.4 | 75.2 | 35.2 | 87.4 | 40.1 |
| CHF | ssROC | 83.2 | 84.9 | 42.0 | 44.1 | 89.2 |
| | supROC | 79.3 | 87.6 | 36.0 | 43.9 | 86.6 |
| ICH | ssROC | 83.6 | 51.3 | 58.5 | 95.8 | 35.4 |
| | supROC | 86.0 | 50.5 | 62.7 | 96.5 | 35.6 |
| SS | ssROC | 85.9 | 75.3 | 49.1 | 74.1 | 75.2 |
| | supROC | 81.6 | 87.7 | 34.1 | 72.4 | 64.1 |
| PD | ssROC | 89.4 | 59.8 | 60.6 | 89.9 | 60.7 |
| | supROC | 87.5 | 66.4 | 52.3 | 89.7 | 53.2 |
| T1DM | ssROC | 90.5 | 80.4 | 68.8 | 57.3 | 93.7 |
| | supROC | 91.5 | 80.0 | 75.0 | 59.8 | 94.8 |

Table 3: **Point estimates for the 6 phenotypes from MGB at a FPR of 10%.**

Figure 5 shows the median RE of supROC to ssROC across the six phenotypes at a FPR

of 10%. The median RE gain across phenotypes and metrics was 1.6, implying that the estimates from ssROC are approximately 40% less variable than supROC on average. Consistent with the simulation findings, the lowest gain was in AUC, with a median RE of 1.4. The most significant RE gain was observed in Threshold, with a median RE of 1.9. These results suggest that the estimates from ssROC for Threshold and AUC are approximately 47% and 29% less variable, respectively, compared to those from supROC. It is important to note that two phenotypes (SS and T1DM) exhibited relatively large RE for the Threshold estimates (Supplementary Figure 2). Supplementary Figure 3 illustrates that the empirical distribution of the resampled estimates for the Threshold from supROC are skewed for SS and multimodal for T1DM, while those from ssROC are approximately normal as expected. This behavior further emphasizes the stability of ssROC relative to supROC in real data.

Consistent with our simulation and theoretical results, we also observe that RE is linked to PA accuracy. For example, a phenotype with high PA accuracy, such as T1DM, exhibits a higher RE compared to CA, which has the lowest PA accuracy. These findings underscore the advantages of our proposed ssROC method compared to its supervised counterpart: ssROC reduces variability of ROC estimates, particularly when the PA score is predictive.

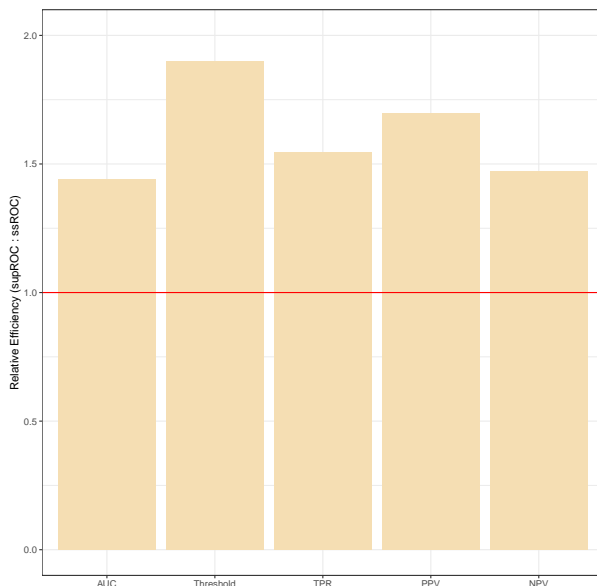


Figure 5: **Median relative efficiency for the 6 phenotypes from MGB at a FPR of 10%.** RE is defined as the ratio of the variance of the estimates from supROC and the variance of the estimates from ssROC.

DISCUSSION

Although high-throughput phenotyping is the backbone of EHR-based research, there is a paucity of methods for reliably evaluating the predictive performance of a PA with limited labeled data. The proposed ssROC method fills this gap. ssROC is a simple two-step estimation procedure that leverages large volumes of unlabeled data by imputing missing gold-standard labels with a nonparametric calibration of a PA score. Unlike existing procedures for PA evaluation in the informatics literature, ssROC eliminates the requirement that the PA be properly calibrated to yield unbiased estimation of the ROC parameters and may be utilized for ML-based PAs [25, 37]. While we focus specifically on weakly-supervised PAs in our theoretical analysis and real data example, given their increasing popularity and ability to automate PA estimation, ssROC can also be used

to evaluate rule-based or other ML-based PAs. Moreover, by harnessing unlabeled data, ssROC yields substantially less variable estimates than supROC in both simulated and real data. Practically, this translates into a significant reduction in the amount of chart review required to obtain a precise understanding of PA performance.

While our work is a first step toward streamlining PA evaluation, there are several avenues that warrant future research. First, ssROC assumes that the labeled examples are randomly sampled from the underlying full data. In situations where the goal is to phenotype multiple conditions or comorbidities, more effective sampling strategies such as stratified random sampling have the potential to further enhance the efficiency of ssROC[53]. However, due to the large discrepancy in size of the labeled and unlabeled data, developing procedures to accommodate non-random sampling is nontrivial [54]. Second, the nonparametric calibration step demands a sufficient amount of labeled data for the kernel regression to be well estimated. Our future work will develop a flexible parametric calibration procedure that accommodates smaller labeled data sizes. Third, ssROC can also be extended for model comparisons and evaluation of fairness metrics, which are urgently needed given the increasing recognition of algorithmic unfairness in informatics applications. The calibration step would need to be augmented in both settings to utilize additional information in multiple PA scores or protected attributes, respectively. This augmentation could potentially lead to a more efficient procedure as ssROC currently only uses information from one PA score for imputation. Lastly, our results demonstrate the ability of ssROC to provide accurate ROC evaluation for six phenotypes with variable prevalence, labeled and unlabeled dataset sizes, and PA performance within one health system. Further work is needed to understand the performance of our method across a diverse range of phenotypes and to extend our approach to accommodate federated

analyses across multiple healthcare systems.

CONCLUSION

In this paper, we introduced a semi-supervised approach, called ssROC, that leverages a large volume of unlabeled data together with a small subset of gold-standard labeled to precisely estimate the ROC parameters of PAs. PA development involves two key steps: (i) algorithm estimation and (ii) algorithm evaluation. While a considerable amount of effort has been placed on algorithm estimation, ssROC fills the current gap in robust and efficient methodology for predictive performance evaluation. Additionally, ssROC is simple to implement and is available in open-source R software to encourage use in practice. When used in conjunction with weakly-supervised PAs, ssROC demonstrates the potential to facilitate the reliable and streamlined phenotyping that is necessary for a wide variety of translational EHR applications.

FUNDING

The project was supported by the Natural Sciences and Engineering Research Council of Canada grant (RGPIN-2021-03734), the University of Toronto Connaught New Researcher Award, and the University of Toronto Seed Funding for Methodologists Grant (to JeG).

AUTHOR CONTRIBUTIONS

JeG conceived and designed the study. JeG, JiG, CB, and CH conducted simulation analyses. CB and CH conducted real data analyses. JeG, JiG, CB, and KZ analyzed and

interpreted the results. JeG and JiG drafted and revised the manuscript. All authors reviewed and approved the final manuscript.

CONFLICT OF INTEREST STATEMENT

The authors have no conflicts of interest to declare.

DATA AND CODE AVAILABILITY

Our proposed method is implemented as an R software package, **ssROC**, which is available at <https://github.com/jlgrons/ssROC>.

REFERENCE

1. McGinnis, J. M., Olsen, L., Goolsby, W. A., *et al.* *Clinical data as the basic staple of health learning: Creating and protecting a public good: Workshop summary* (National Academies Press, 2011).
2. Boockvar, K. S., Livote, E. E., Goldstein, N., *et al.* Electronic health records and adverse drug events after patient transfer. *Quality and Safety in Health Care* **19**, e16–e16 (2010).
3. Kurreeman, F., Liao, K., Chibnik, L., *et al.* Genetic basis of autoantibody positive and negative rheumatoid arthritis risk in a multi-ethnic cohort derived from electronic health records. *The American Journal of Human Genetics* **88**, 57–69 (2011).

4. Liao, K. P., Kurreeman, F., Li, G., *et al.* Associations of autoantibodies, autoimmune risk alleles, and clinical diagnoses from the electronic medical records in rheumatoid arthritis cases and non-rheumatoid arthritis controls. *Arthritis & Rheumatism* **65**, 571–581 (2013).
5. Chen, C.-Y., Lee, P. H., Castro, V. M., *et al.* Genetic validation of bipolar disorder identified by automated phenotyping using electronic health records. *Translational psychiatry* **8**, 1–8 (2018).
6. Li, R., Chen, Y., Ritchie, M. D., *et al.* Electronic health records and polygenic risk scores for predicting disease risk. *Nature Reviews Genetics*, 1–10 (2020).
7. Brat, G. A., Weber, G. M., Gehlenborg, N., *et al.* International electronic health record-derived COVID-19 clinical course profiles: the 4CE consortium. *NPJ digital medicine* **3**, 1–9 (2020).
8. Bastarache, L. Using phecodes for research with the electronic health record: from PheWAS to PheRS. *Annual review of biomedical data science* **4**, 1–19 (2021).
9. Prieto-Alhambra, D., Kostka, K., Duarte-Salles, T., *et al.* Unraveling COVID-19: a large-scale characterization of 4.5 million COVID-19 cases using CHARYBDIS. *Research square* (2021).
10. Henry, K. E., Adams, R., Parent, C., *et al.* Factors driving provider adoption of the TREWS machine learning-based early warning system and its effects on sepsis treatment timing. *Nature medicine* **28**, 1447–1454 (2022).
11. Shivade, C., Raghavan, P., Fosler-Lussier, E., *et al.* A review of approaches to identifying patient phenotype cohorts using electronic health records. *Journal of the American Medical Informatics Association* **21**, 221–230 (2014).

12. Banda, J. M., Seneviratne, M., Hernandez-Boussard, T., *et al.* Advances in electronic phenotyping: from rule-based definitions to machine learning models. *Annual review of biomedical data science* **1**, 53 (2018).
13. Alzoubi, H., Alzubi, R., Ramzan, N., *et al.* A review of automatic phenotyping approaches using electronic health records. *Electronics* **8**, 1235 (2019).
14. Yang, S., Varghese, P., Stephenson, E., *et al.* Machine learning approaches for electronic health records phenotyping: a methodical review. *Journal of the American Medical Informatics Association* **30**, 367–381 (2023).
15. Zhang, Y., Cai, T., Yu, S., *et al.* High-throughput phenotyping with electronic medical record data using a common semi-supervised approach (PheCAP). *Nature Protocols* **14**, 3426–3444 (2019).
16. Murphy, S., Churchill, S., Bry, L., *et al.* Instrumenting the health care enterprise for discovery research in the genomic era. *Genome research* **19**, 1675–1681 (2009).
17. Castro, V., Shen, Y., Yu, S., *et al.* Identification of subjects with polycystic ovary syndrome using electronic health records. *Reproductive Biology and Endocrinology* **13**, 116 (2015).
18. Teixeira, P. L., Wei, W.-Q., Cronin, R. M., *et al.* Evaluating electronic health record data sources and algorithmic approaches to identify hypertensive individuals. *Journal of the American Medical Informatics Association* **24**, 162–171 (Jan. 2017).
19. Geva, A., Gronsbell, J. L., Cai, T., *et al.* A computable phenotype improves cohort ascertainment in a pediatric pulmonary hypertension registry. *The Journal of pediatrics* **188**, 224–231 (2017).

20. Meaney, C., Widdifield, J., Jaakkimainen, L., *et al.* Using Biomedical Text as Data and Representation Learning for Identifying Patients with an Osteoarthritis Phenotype in the Electronic Medical Record. *International Journal of Population Data Science* **3** (2018).
21. Gehrman, S., Derroncourt, F., Li, Y., *et al.* Comparing deep learning and concept extraction based methods for patient phenotyping from clinical narratives. *PLOS ONE* **13** (ed Chuang, J.-H.) e0192360 (Feb. 2018).
22. Liao, K. P., Sun, J., Cai, T. A., *et al.* High-throughput multimodal automated phenotyping (MAP) with application to PheWAS. *Journal of the American Medical Informatics Association* **26**, 1255–1262 (2019).
23. Nori, V. S., Hane, C. A., Sun, Y., *et al.* Deep neural network models for identifying incident dementia using claims and EHR datasets. *PLOS ONE* **15** (ed Chen, K.) e0236400 (Sept. 2020).
24. Ni, Y., Bachtel, A., Nause, K., *et al.* Automated detection of substance use information from electronic health records for a pediatric population. *Journal of the American Medical Informatics Association* **28**, 2116–2127 (2021).
25. Swerdel, J. N., Hripcsak, G. & Ryan, P. B. PheValuator: development and evaluation of a phenotype algorithm evaluator. *Journal of biomedical informatics* **97**, 103258 (2019).
26. Chartier, C., Gfrerer, L. & Austen, W. G. ChartSweep: A HIPAA-compliant Tool to Automate Chart Review for Plastic Surgery Research. *Plastic and Reconstructive Surgery - Global Open* **9**, e3633. (2023) (2021).

27. Yu, S., Liao, K. P., Shaw, S. Y., *et al.* Toward high-throughput phenotyping: unbiased automated feature extraction and selection from knowledge sources. *Journal of the American Medical Informatics Association* **22**, 993–1000 (2015).
28. Yu, S., Chakraborty, A., Liao, K. P., *et al.* Surrogate-assisted feature extraction for high-throughput phenotyping. *Journal of the American Medical Informatics Association* **24**, e143–e149 (2017).
29. Nogues, I.-E., Wen, J., Lin, Y., *et al.* Weakly Semi-supervised phenotyping using Electronic Health records. *Journal of Biomedical Informatics* **134**, 104175 (2022).
30. Wright, A., Chen, E. S. & Maloney, F. L. An automated technique for identifying associations between medications, laboratory results and problems. *Journal of biomedical informatics* **43**, 891–901 (2010).
31. Wright, A., Pang, J., Feblowitz, J. C., *et al.* A method and knowledge base for automated inference of patient problems from structured data in an electronic medical record. *Journal of the American Medical Informatics Association* **18**, 859–867 (2011).
32. Agarwal, V., Podchiyska, T., Banda, J. M., *et al.* Learning statistical models of phenotypes using noisy labeled training data. *Journal of the American Medical Informatics Association* **23**, 1166–1173 (2016).
33. Banda, J. M., Halpern, Y., Sontag, D., *et al.* Electronic phenotyping with APHRODITE and the Observational Health Sciences and Informatics (OHDSI) data network. *AMIA Summits on Translational Science Proceedings* **2017**, 48 (2017).
34. Huang, J., Duan, R., Hubbard, R. A., *et al.* PIE: A prior knowledge guided integrated likelihood estimation method for bias reduction in association studies using electronic

- health records data. *Journal of the American Medical Informatics Association* **25**, 345–352 (2018).
35. Tong, J., Huang, J., Chubak, J., *et al.* An augmented estimation procedure for EHR-based association studies accounting for differential misclassification. *Journal of the American Medical Informatics Association* **27**, 244–253 (2020).
 36. Yin, Z., Tong, J., Chen, Y., *et al.* A cost-effective chart review sampling design to account for phenotyping error in electronic health records (EHR) data. *Journal of the American Medical Informatics Association* **29**, 52–61 (2022).
 37. Swerdel, J. N., Schuemie, M., Murray, G., *et al.* PheValuator 2.0: Methodological improvements for the PheValuator approach to semi-automated phenotype algorithm evaluation. *Journal of Biomedical Informatics* **135**, 104177 (2022).
 38. Gronsbell, J. L. & Cai, T. Semi-supervised approaches to efficient evaluation of model prediction performance. *Journal of the Royal Statistical Society: Series B (Statistical Methodology)* **80**, 579–594 (2018).
 39. Gronsbell, J., Liu, M., Tian, L., *et al.* Efficient estimation and evaluation of prediction rules in semi-supervised settings under stratified sampling. *arXiv preprint arXiv:2010.09443* (2020).
 40. Van Calster, B., McLernon, D. J., Van Smeden, M., *et al.* Calibration: the Achilles heel of predictive analytics. *BMC medicine* **17**, 1–7 (2019).
 41. Huang, Y., Li, W., Macheret, F., *et al.* A tutorial on calibration measurements and calibration models for clinical prediction models. *Journal of the American Medical Informatics Association* **27**, 621–633 (2020).
 42. Pepe, M. S. *The statistical evaluation of medical tests for classification and prediction* (Oxford University Press, 2003).

43. Cai, T. & Moskowitz, C. S. Semi-parametric estimation of the binormal ROC curve for a continuous diagnostic test. *Biostatistics* **5**, 573–586 (2004).
44. Jin, Z., Ying, Z. & Wei, L. A Simple Resampling Method by Perturbing the Minimax. *Biometrika* **88**, 381–390 (June 2001).
45. Bertail, P., Cléménçon, S. & Vayatis, N. On bootstrapping the ROC curve. *Advances in Neural Information Processing Systems* **21** (2008).
46. Denny, J. C., Bastarache, L., Ritchie, M. D., *et al.* Systematic comparison of phenome-wide association study of electronic medical record data and genome-wide association study data. *Nature biotechnology* **31**, 1102–1111 (2013).
47. Yu, S., Ma, Y., Gronsbell, J., *et al.* Enabling phenotypic big data with PheNorm. *Journal of the American Medical Informatics Association* **25**, 54–60 (2018).
48. Lindberg, D. A., Humphreys, B. L. & McCray, A. T. The unified medical language system. *Yearbook of medical informatics* **2**, 41–51 (1993).
49. Yu, S., Cai, T. & Cai, T. NILE: fast natural language processing for electronic health records. *arXiv preprint arXiv:1311.6063* (2013).
50. Wand, M. P., Marron, J. S. & Ruppert, D. Transformations in density estimation. *Journal of the American Statistical Association* **86**, 343–353 (1991).
51. Sinnott, J. A. & Cai, T. Inference for survival prediction under the regularized Cox model. *Biostatistics* **17**, 692–707 (2016).
52. Agresti, A. *Categorical data analysis* (John Wiley & Sons, 2012).
53. Tan, W. K. & Heagerty, P. J. Surrogate-guided sampling designs for classification of rare outcomes from electronic medical records data. *Biostatistics* **23**, 345–361 (2022).

54. Zhang, Y., Chakraborty, A. & Bradic, J. *Double Robust Semi-Supervised Inference for the Mean: Selection Bias under MAR Labeling with Decaying Overlap* May 2023. arXiv: 2104.06667 [math, stat].

ssROC: Semi-Supervised ROC Analysis for Reliable and Streamlined Evaluation of Phenotyping Algorithms

Jianhui Gao[†], Clara-Lea Bonzel[†], Chuan Hong,
Paul Varghese, Karim Zakir, Jessica Gronsbell*

[†] These authors contributed equally.

*Correspondence: j.gronsbell@utoronto.ca.

Contents

| | | |
|----------|--|-----------|
| 1 | Technical Detail of ssROC | 1 |
| 2 | Inference Procedure for ssROC | 1 |
| 2.1 | Perturbation Resampling Procedure | 1 |
| 2.2 | Construction of Confidence Intervals (CIs) | 3 |
| 3 | Theoretical Properties of ssROC and supROC | 5 |
| 3.1 | Proof of Theorem 1 | 8 |
| 3.1.1 | Supervised Estimator | 8 |
| 3.2 | Semi-supervised Estimator | 12 |
| 4 | Description of the PheNorm Algorithm | 17 |
| 5 | Simulation Study | 19 |

6 Analysis of 6 PAs from MGB **21**

6.1 Relative Efficiency 21

6.2 Perturbation Resampling 22

1 Technical Detail of ssROC

We provide a detailed description of the two steps in our proposed ssROC method. In step I, we estimate $m(s) = P(Y = 1 | S = s)$ with \mathcal{L} via local constant regression as

$$\widehat{m}(s) = \frac{\sum_{i=1}^n K_h(S_i - s) Y_i}{\sum_{i=1}^n K_h(S_i - s)}$$

where $K_h(u) = h^{-1}K(u/h)$ is a given smooth, symmetric kernel function, h is a bandwidth controlling the smoothing, and $nh^2 \rightarrow \infty$ and $nh^4 \rightarrow 0$ as $n \rightarrow \infty$. The conditions on the bandwidth h ensure that $\widehat{m}(s)$ is undersmoothed to prevent bias in the estimated ROC parameters. The estimator $\widehat{m}(s)$ is simply a weighted average of observed labels Y with the weights determined by the kernel function. In step II, the imputed values $\widehat{m}(s)$ in \mathcal{U} are used in place of gold-standard labels Y to estimate the ROC parameters. For example, the semi-supervised estimator for the TPR and FPR are

$$\widehat{\text{TPR}}_{\text{ssROC}}(c) = \frac{\sum_{i=n+1}^{n+N} \widehat{m}(S_i) I(S_i > c)}{\sum_{i=n+1}^{n+N} \widehat{m}(S_i)} \quad \text{and} \quad \widehat{\text{FPR}}_{\text{ssROC}}(c) = \frac{\sum_{i=n+1}^{n+N} [1 - \widehat{m}(S_i)] I(S_i > c)}{\sum_{i=n+1}^{n+N} [1 - \widehat{m}(S_i)]}.$$

2 Inference Procedure for ssROC

We detail the perturbation resampling procedure for obtaining standard error estimates and describe the construction of the corresponding confidence (CI) interval.

2.1 Perturbation Resampling Procedure

Perturbation resampling involves obtaining a large number, B , of perturbed estimates of the parameter of interest by re-weighting the observations according to independently and identically distributed non-negative weights generated independently from the data

and from a distribution with unit mean and variance [1]. Perturbation can be thought of as a smoothed version of traditional bootstrap resampling. In a bootstrap resample, one is essentially re-weighting each observation by weight from a multinomial random variable with the number of trials equal to the sample size and the probabilities all equal to the inverse of the sample size. Perturbation resampling can exhibit improved coverage relative to the traditional bootstrap using weights from a distribution of a continuous random variable [1].

Specifically, we let $\mathcal{G}^{(b)} = \{G_1^{(b)}, \dots, G_n^{(b)}, G_{n+1}^{(b)}, \dots, G_{n+N}^{(b)}\}$ be a set of independent and identically distributed positive random variables with unit mean and variance for $b = 1, \dots, B$. Using the TPR for illustration, perturbation resampling involves iterating the following procedure B times:

Step I. Obtain a perturbed estimate of the $m(s) = P(Y = 1 | S = s)$ as

$$\widehat{m}^{(b)}(s) = \frac{\sum_{i=1}^n K_h(S_i - s) Y_i G_i^{(b)}}{\sum_{i=1}^n K_h(S_i - s) G_i^{(b)}}$$

using the same kernel and bandwidth for the original data.

Step II. Obtain a perturbed estimate of the TPR as

$$\widehat{\text{TPR}}_{ss\text{ROC}}^{(b)}(c) = \frac{\sum_{i=n+1}^{n+N} \widehat{m}^{(b)}(S_i) I(S_i > c) G_i^{(b)}}{\sum_{i=n+1}^{n+N} \widehat{m}^{(b)}(S_i) G_i^{(b)}}.$$

The same procedure can be applied to all of the ROC parameters. Additionally, it is important to note that theoretically one does not need to apply weights to Step II as we assume $n \gg N$. This assumption implies that integrating over the empirical distribution of the PA scores in the unlabeled set does not contribute to the overall variation in the ROC parameter estimates [2]. However, we found that using weights for both Step I and Step II provided improved coverage in our simulation studies. We used an analogous

procedure for supROC.

2.2 Construction of Confidence Intervals (CIs)

Analogous to bootstrap resampling, the standard error estimates ($\widehat{\text{se}}$) are obtained with the standard deviation of the B perturbed TPR parameter estimates as

$$\widehat{\text{se}} \left[\widehat{\text{TPR}}_{ssROC}(c) \right] = \sqrt{\frac{1}{B-1} \sum_{b=1}^B \left[\widehat{\text{TPR}}_{ssROC}^{(b)}(c) - \frac{1}{B} \sum_{b=1}^B \widehat{\text{TPR}}_{ssROC}^{(b)}(c) \right]^2}.$$

Relying on the normal approximation to the sampling distribution of the ssROC estimator of the TPR, a standard Wald $100(1 - \alpha)\%$ CI can be constructed accordingly as $\widehat{\text{TPR}}_{ssROC}(c) \pm z_{1-\alpha/2} \times \widehat{\text{se}} \left[\widehat{\text{TPR}}_{ssROC}(c) \right]$. We verify in the next section that all of the ssROC parameters are asymptotically normal.

However, analogously to supervised estimation, the sampling distribution of the ROC parameters are often skewed when the size of the labeled data is not large [3]. Logit-based intervals can improve the coverage of the CI. The logit-based intervals are obtained by applying a logit transformation to the resampled estimates, computing a Wald-based interval with the transformed estimates, and then converting the upper and lower confidence bounds back to the original scale.

Specifically, we apply $\text{logit}(x) = \log\left(\frac{x}{1-x}\right)$ to $\widehat{\text{TPR}}_{ssROC}(c)$, and a $100(1 - \alpha)\%$ Wald CI of $\text{logit} \left[\widehat{\text{TPR}}_{ssROC}(c) \right]$ is

$$\text{logit} \left[\widehat{\text{TPR}}_{ssROC}(c) \right] \pm z_{1-\alpha/2} \times \widehat{\text{se}} \left\{ \text{logit} \left[\widehat{\text{TPR}}_{ssROC}(c) \right] \right\},$$

where $\widehat{\text{se}} \left\{ \text{logit} \left[\widehat{\text{TPR}}_{ssROC}(c) \right] \right\}$ is the standard deviation of the B perturbed logit transformed estimates. To obtain a $100(1 - \alpha)\%$ CI for $\widehat{\text{TPR}}_{ssROC}(c)$, we convert the upper

and lower confidence bounds back by

$$\text{logit}^{-1} \left\{ \text{logit} \left[\widehat{\text{TPR}}_{ssROC}(c) \right] \pm z_{1-\alpha/2} \times \widehat{\text{se}} \left\{ \text{logit} \left[\widehat{\text{TPR}}_{ssROC}(c) \right] \right\} \right\},$$

where $\text{logit}^{-1}(x) = \frac{1}{1+\exp(-x)}$. We recommend the use the logit-based interval as it performed best overall in terms of coverage probability in our simulation studies.

3 Theoretical Properties of ssROC and supROC

We present the asymptotic distributions of ssROC and supROC and also compare their asymptotic variances to establish the improved precision of ssROC relative to supROC. The consistency of both estimators follows from [2]. Most of our assumptions are adopted from [2], which are restated below.

Assumption 1 (Semi-supervised setting). *We assume that: (i) $\mathcal{L} \perp\!\!\!\perp \mathcal{U}$, (ii) $N \gg n$ so that $n/N \rightarrow 0$ as $n \rightarrow \infty$, and (iii) the labels are missing completely at random.*

Assumption 2 (Modeling Assumptions for the Phenotyping Algorithm (PA) score). *We assume that the PA score is derived from a working parametric model fit with \mathcal{U} . The model is parameterized by a p -dimensional parameter, $\boldsymbol{\theta}$, for some fixed p . Let $\hat{\boldsymbol{\theta}}$ be the estimator obtained from the fitting with \mathcal{U} and let $\boldsymbol{\theta}^*$ be the limiting value of $\hat{\boldsymbol{\theta}}$ where $\boldsymbol{\theta}^*$ belongs to a compact parameter space. We assume that $\hat{\boldsymbol{\theta}}$ is asymptotically linear with*

$$\sqrt{N}(\hat{\boldsymbol{\theta}} - \boldsymbol{\theta}^*) = N^{-1/2} \sum_{i=1}^N U(\mathbf{Z}_i) + o_p(1)$$

where \mathbf{Z}_i denotes the data used for algorithm estimation, $U(\cdot)$ is a deterministic function with $\| \text{Var}[U(\mathbf{Z}_i)] \| < \infty$ and $E[U(\mathbf{Z}_i)] = 0$. For ease of notation and consistency with the main text, we denote the estimated PA score as $S = S_{\hat{\boldsymbol{\theta}}} = S(\mathbf{Z}; \hat{\boldsymbol{\theta}})$ and the limiting PA score $S^* = S_{\boldsymbol{\theta}^*} = S(\mathbf{Z}; \boldsymbol{\theta}^*)$. We assume that S^* is a continuous random variable with continuously differentiable density function, $f(s)$, with bounded support.

Remark. The assumptions on the model used to obtain the PA are quite flexible and include a wide range of commonly used parametric models. For example, many parametric mixture models satisfy Assumption 2 [4, 5]. Noisy-label regression models, such as those in APHRODITE, also satisfy Assumption 2 [6, 7].

Assumption 3 (Regularity conditions for kernel smoothing). *We assume that: (i) $K(\cdot)$ is a symmetric q th order kernel for some integer $q \geq 2$ that is bounded and Lipschitz*

continuous, (ii) for some $\epsilon > 0$, $E|Y|^{2+\epsilon} < \infty$ and $\sup_s \int |y|^{2+\epsilon} f(y | s) f(s) dy < \infty$, and (iii) the bandwidth h satisfies $\frac{\log(n)}{n^{1/2}h} \rightarrow 0$ and $n^{1/2}h^2 \rightarrow 0$.

Assumption 4 (Assumptions for ROC analysis). *We assume that for any classification threshold c , the gradient vectors $\nabla_{\theta} \text{TPR}(c)$ and $\nabla_{\theta} \text{FPR}(c)$ exist and are continuous in an open neighbourhood containing θ^* .*

The subsequent discussions are abbreviated versions of the arguments provided in [2] and are provided to facilitate our comparison of ssROC relative to supROC. The primary difference in our analysis is that we assume a more flexible working model based on a weakly-supervised estimation, while [2] assumes a supervised penalized logistic regression model with the ALASSO penalty.

We provide the influence function for a point along the ROC curve, $\text{ROC}(u_0) = \text{TPR}(c_{u_0})$ where $c_{u_0} = \text{FPR}^{-1}(u_0)$. The corresponding ssROC and supROC are denoted respectively as

$$\widehat{\text{ROC}}_{\text{ssROC}}(u_0) = \widehat{\text{TPR}}_{\text{ssROC}}(\tilde{c}_{u_0}) = \widehat{\text{TPR}}_{\text{ssROC}} \left[\widehat{\text{FPR}}_{\text{ssROC}}^{-1}(u_0) \right]$$

and

$$\widehat{\text{ROC}}_{\text{supROC}}(u_0) = \widehat{\text{TPR}}_{\text{supROC}}(\hat{c}_{u_0}) = \widehat{\text{TPR}}_{\text{supROC}} \left[\widehat{\text{FPR}}_{\text{supROC}}^{-1}(u_0) \right].$$

Our main result is provided in the following theorem.

Theorem 1. *Under Assumption 1 – 4,*

$$\begin{aligned} \widetilde{\mathcal{W}}_{\text{ROC}}(u_0) &= n^{1/2} \left[\widehat{\text{ROC}}_{\text{ssROC}}(u_0) - \text{ROC}(u_0) \right] \\ &= n^{-1/2} \sum_{i=1}^n \mathcal{G}_i(S; \theta^*, c_{u_0}) [Y_i - m(S_i^*)] + o_p(1) \end{aligned}$$

and

$$\begin{aligned}\widehat{W}_{ROC}(u_0) &= n^{1/2} \left[\widehat{ROC}_{supROC}(u_0) - ROC(u_0) \right] \\ &= n^{-1/2} \sum_{i=1}^n [\mathcal{G}_i(S; \boldsymbol{\theta}^*, c_{u_0})(Y_i - \mu) + \Gamma_i(S; \boldsymbol{\theta}^*, c_{u_0})] + o_p(1),\end{aligned}$$

where $\mu = P(Y = 1)$, $R\dot{O}C(u_0) = \frac{\partial ROC(u)}{\partial u}|_{u=u_0}$, $\mathcal{G}_i(S; \boldsymbol{\theta}^*, c_{u_0}) = \left[\mu^{-1} + \mu_0^{-1} R\dot{O}C(u_0) \right] I(S_i^* \geq c_{u_0}) - \left[\mu^{-1} ROC(u_0) + \mu_0^{-1} R\dot{O}C(u_0) u_0 \right]$, and $\Gamma_i(S; \boldsymbol{\theta}^*, c_{u_0}) = I(S_i^* \geq c_{u_0}) - ROC(u_0) - R\dot{O}C(u_0)[I(S_i^* \geq c_{u_0}) - u_0]$.

Remark. Theorem 1 provides the influence functions for the ssROC and supROC estimators. Standard asymptotic theory guarantees both estimators are asymptotically normal with mean $ROC(u_0)$ and variances determined by their influence functions [8]. We use $a\text{Var} \left[\widetilde{ROC}_{ssROC}(u_0) \right]$ and $a\text{Var} \left[\widehat{ROC}_{supROC}(u_0) \right]$ to denote the corresponding asymptotic variances.

Remark. The improvements in $a\text{Var} \left[\widetilde{ROC}_{ssROC}(u_0) \right]$ relative to $a\text{Var} \left[\widehat{ROC}_{supROC}(u_0) \right]$ can be understood from the influence functions in Theorem 1. Specifically, the influence function for ssROC is centered at the conditional mean $m(S_i^*) = P(Y_i = 1 | S_i^*)$ whereas the influence function of supROC is centered at the marginal mean $\mu = P(Y = 1)$. The influence function for supROC also has an extra non-vanishing term $\Gamma_i(S; \boldsymbol{\theta}^*, c_{u_0})$. These differences yield a reduction in the asymptotic variance of ssROC. Additionally, this result differs from that of [2] as the estimated model parameter, $\widehat{\boldsymbol{\theta}}$, converges at a rate of \sqrt{N} . The variation from estimating $\boldsymbol{\theta}^*$ with $\widehat{\boldsymbol{\theta}}$ is therefore asymptotically negligible at the \sqrt{n} rate and hence the proposed semi-supervised estimator *always* has asymptotic variance smaller than that of supROC. Details are provided in Corollary 1.1.

Corollary 1.1. Let $\mathcal{G}(S; \boldsymbol{\theta}^*, c_{u_0}) = \left[\mu^{-1} + \mu_0^{-1} R\dot{O}C(u_0) \right] I(S^* \geq c_{u_0}) - \left[\mu^{-1} ROC(u_0) + \mu_0^{-1} R\dot{O}C(u_0) u_0 \right]$, and $\Gamma(S; \boldsymbol{\theta}^*, c_{u_0}) = I(S^* \geq c_{u_0}) - ROC(u_0) - R\dot{O}C(u_0)[I(S^* \geq c_{u_0}) - u_0]$,

then

$$\begin{aligned}\Delta_v^{asy}(u_0) &:= n \left\{ a \text{Var} \left[\widehat{\text{ROC}}_{supROC}(u_0) \right] - a \text{Var} \left[\widetilde{\text{ROC}}_{ssROC}(u_0) \right] \right\} \\ &= \text{Var} \{ \mathcal{G}(S; \boldsymbol{\theta}^*, c_{u_0}) [m(S^*) - \mu] + \Gamma(S; \boldsymbol{\theta}^*, c_{u_0}) \} \geq 0.\end{aligned}$$

Proof. By the law of total variance,

$$\begin{aligned}n \left\{ a \text{Var} \left[\widehat{\text{ROC}}_{supROC}(c_{u_0}) \right] \right\} &= \\ \text{E} \{ [\mathcal{G}(S; \boldsymbol{\theta}^*, c_{u_0})]^2 \text{Var}(Y|S^*) \} &+ \text{Var} \{ \mathcal{G}(S; \boldsymbol{\theta}^*, c_{u_0}) [m(S^*) - \mu] + \Gamma(S; \boldsymbol{\theta}^*, c_{u_0}) \},\end{aligned}$$

and

$$n \left\{ a \text{Var} \left[\widetilde{\text{ROC}}_{ssROC}(c_{u_0}) \right] \right\} = \text{E} \{ [\mathcal{G}(S; \boldsymbol{\theta}^*, c_{u_0})]^2 \text{Var}(Y|S^*) \}.$$

Hence,

$$\begin{aligned}\Delta_v^{asy}[\text{ROC}(u_0)] &:= n \left\{ a \text{Var} \left[\widehat{\text{ROC}}_{supROC}(u_0) \right] - a \text{Var} \left[\widetilde{\text{ROC}}_{ssROC}(u_0) \right] \right\} \\ &= \text{Var} \{ \mathcal{G}(S; \boldsymbol{\theta}^*, c_{u_0}) [m(S^*) - \mu] + \Gamma(S; \boldsymbol{\theta}^*, c_{u_0}) \} \geq 0.\end{aligned}$$

□

3.1 Proof of Theorem 1

3.1.1 Supervised Estimator

Following the arguments of [2], $\widehat{\text{ROC}}_{supROC}(u_0)$ is consistent for $\text{ROC}(u_0)$ and $\sup_{u_0 \in [0,1]} |\hat{c}_u - c_{u_0}| = o_p(1)$, where $c_{u_0} = \text{FPR}^{-1}(u_0)$, $\hat{c}_u = \widehat{\text{FPR}}_{supROC}^{-1}(u_0)$. To establish the weak con-

vergence of $\widehat{\mathcal{W}}_{\text{ROC}}(u_0) = n^{1/2} \left[\widehat{\text{ROC}}_{\text{supROC}}(u_0) - \text{ROC}(u_0) \right]$, we note that

$$\begin{aligned} \widehat{\mathcal{W}}_{\text{ROC}}(u_0) &= n^{1/2} \left\{ \widehat{\text{TPR}}_{\text{supROC}} \left[\widehat{\text{FPR}}_{\text{supROC}}^{-1}(u_0) \right] - \text{TPR} \left[\text{FPR}^{-1}(u_0) \right] \right\} \\ &= n^{1/2} \left[\widehat{\text{TPR}}_{\text{supROC}}(\hat{c}_u) - \text{TPR}(c_{u_0}) \right] \\ &= n^{1/2} \left[\widehat{\text{TPR}}_{\text{supROC}}(\hat{c}_u) - \text{TPR}(\hat{c}_u) \right] + n^{1/2} [\nabla_c \text{TPR}(c_{u_0})(\hat{c}_u - c_{u_0})] + o_p(1) \\ &= \widehat{\mathcal{W}}_{\text{TPR}}(\hat{c}_u) - \text{ROC}(u_0) \widehat{\mathcal{W}}_{\text{FPR}}(\hat{c}_u) + o_p(1) \end{aligned}$$

where $\text{ROC}(u_0) = \frac{\partial \text{ROC}(u_0)}{\partial u_0}$, $\widehat{\mathcal{W}}_{\text{TPR}}(c) = n^{1/2} \left[\widehat{\text{TPR}}_{\text{supROC}}(c) - \text{TPR}(c) \right]$, $\widehat{\mathcal{W}}_{\text{FPR}}(c) = n^{1/2} \left[\widehat{\text{FPR}}_{\text{supROC}}(c) - \text{FPR}(c) \right]$.

It therefore suffices to utilize the two steps outlined in Figure 1 to show that $\widehat{\mathcal{W}}_{\text{ROC}}(u_0)$ converges weakly to a zero-mean Gaussian distribution.

Key Steps

Step 1. Show that $\widehat{\mathcal{W}}_{\text{TPR}}(c)$ converges weakly to a zero mean Gaussian process.

Step 2. Show that $\widehat{\mathcal{W}}_{\text{FPR}}(c)$ converges weakly to a zero mean Gaussian process.

Figure 1: **Overview of the Proof**

Throughout we let g be a measurable function define $\mathbb{P}_n g = n^{-1} \sum_{i=1}^n g(X_i)$, $\mathbb{P}g = \int g dP$, and $\mathbb{G}_n g = n^{1/2}(\mathbb{P}_n g - \mathbb{P}g)$ be the scaled empirical process indexed by g .

Step 1: Weak convergence of $\widehat{\mathcal{W}}_{\text{TPR}}(c)$

We decompose $\widehat{\mathcal{W}}_{\text{TPR}}(c)$ into

$$\begin{aligned}\widehat{\mathcal{W}}_{\text{TPR}}(c) &= n^{1/2} \left[\widehat{\text{TPR}}_{\text{supROC}}(c; \widehat{\boldsymbol{\theta}}) - \text{TPR}(c; \widehat{\boldsymbol{\theta}}) \right] + n^{1/2} \left[\text{TPR}(c; \widehat{\boldsymbol{\theta}}) - \text{TPR}(c; \boldsymbol{\theta}^*) \right] \\ &= n^{1/2} \left[\widehat{\text{TPR}}_{\text{supROC}}(c; \widehat{\boldsymbol{\theta}}) - \text{TPR}(c; \widehat{\boldsymbol{\theta}}) \right] + n^{1/2} \nabla_{\boldsymbol{\theta}} \text{TPR}(c, \boldsymbol{\theta}^*) (\widehat{\boldsymbol{\theta}} - \boldsymbol{\theta}^*) + o_p(1)\end{aligned}\tag{1}$$

The second term of (1), which accounts for the variation in estimating $\boldsymbol{\theta}^*$, converges in probability to zero as $N^{1/2}(\widehat{\boldsymbol{\theta}} - \boldsymbol{\theta}^*) = O_p(1)$ and thus

$$n^{1/2} \nabla_{\boldsymbol{\theta}} \text{TPR}(c, \boldsymbol{\theta}^*) (\widehat{\boldsymbol{\theta}} - \boldsymbol{\theta}^*) = O_p[(n/N)^{1/2}] = o_p(1)$$

by Assumptions 1 and 2.

For the first term of (1), define $\widehat{\xi}(c, \boldsymbol{\theta}) = n^{-1} \sum_{i=1}^n I(S_{\boldsymbol{\theta}, i} \geq c) Y_i$, $\xi(c, \boldsymbol{\theta}) = \text{E}[I(S_{\boldsymbol{\theta}} \geq c) Y]$, and

$$\widehat{\mathcal{W}}_{\xi}(c, \boldsymbol{\theta}) = n^{1/2} \left[\widehat{\xi}(c, \boldsymbol{\theta}) - \xi(c, \boldsymbol{\theta}) \right] = \mathbb{G}_n[I(S_{\boldsymbol{\theta}} \geq c) Y].$$

Then,

$$\begin{aligned}n^{1/2} \left[\widehat{\text{TPR}}_{\text{supROC}}(c; \boldsymbol{\theta}) - \text{TPR}(c; \boldsymbol{\theta}) \right] &= n^{1/2} \left[\frac{\widehat{\xi}(c, \boldsymbol{\theta})}{\widehat{\xi}(0, \boldsymbol{\theta})} - \frac{\xi(c, \boldsymbol{\theta})}{\xi(0, \boldsymbol{\theta})} \right] \\ &= n^{1/2} \left\{ \frac{\widehat{\xi}(c, \boldsymbol{\theta}) - \xi(c, \boldsymbol{\theta})}{\widehat{\xi}(0, \boldsymbol{\theta})} + \xi(c, \boldsymbol{\theta}) \left[\frac{1}{\widehat{\xi}(0, \boldsymbol{\theta})} - \frac{1}{\xi(0, \boldsymbol{\theta})} \right] \right\} \\ &= \mu^{-1} \left[\widehat{\mathcal{W}}_{\xi}(c, \boldsymbol{\theta}) - \text{TPR}(c; \boldsymbol{\theta}) \widehat{\mathcal{W}}_{\xi}(0, \boldsymbol{\theta}) \right] \frac{\xi(0, \boldsymbol{\theta})}{\widehat{\xi}(0, \boldsymbol{\theta})},\end{aligned}$$

where $\mu = \text{E}(Y) = \xi(0, \boldsymbol{\theta})$.

By the uniform law of large numbers (ULLN) [Lemma 2.4, 9], $\sup_{\boldsymbol{\theta} \in \Theta} |\widehat{\xi}(c, \boldsymbol{\theta}) - \xi(c, \boldsymbol{\theta})| \xrightarrow{p} 0$

and $\xi(0, \boldsymbol{\theta})/\widehat{\xi}(0, \boldsymbol{\theta}) \xrightarrow{p} 1$. To establish the weak convergence of $\widehat{\mathcal{W}}_\xi(c, \boldsymbol{\theta})$, consider the class of functions

$$\{I(S_{\boldsymbol{\theta}} \geq c) : \boldsymbol{\theta} \in \Theta, c \in [0, 1]\}$$

which is a Vapnik-Chervonenkis class [Example 19.16, 10]. It follows that

$$\widehat{\mathcal{W}}_\xi(c, \boldsymbol{\theta}) = n^{-1/2} \sum_{i=1}^n [Y_i I(S_{\boldsymbol{\theta}, i} \geq c) - \mu \text{TPR}(c; \boldsymbol{\theta})]$$

converges weakly to a mean zero Gaussian process indexed by $(\boldsymbol{\theta}, c)$ and is stochastic equicontinuous in $(\boldsymbol{\theta}, c)$ so that

$$\begin{aligned} \widehat{\mathcal{W}}_{\text{TPR}}(c) &= \mu^{-1} \left[\widehat{\mathcal{W}}_\xi(c, \boldsymbol{\theta}^*) - \text{TPR}(c) \widehat{\mathcal{W}}_\xi(0, \boldsymbol{\theta}^*) \right] + o_p(1) \\ &= \mu^{-1} \left\{ n^{-1/2} \sum_{i=1}^n Y_i [I(S_i^* \geq c) - \text{TPR}(c)] \right\} + o_p(1) \\ &= n^{-1/2} \sum_{i=1}^n \mu^{-1} \{ (Y_i - \mu) [I(S_i^* \geq c) - \text{TPR}(c)] + \mu [I(S_i^* \geq c) - \text{TPR}(c)] \} + o_p(1). \end{aligned}$$

Step 2: Weak convergence of $\widehat{\mathcal{W}}_{\text{FPR}}(c)$

Let $\widehat{\zeta}(c, \boldsymbol{\theta}) = n^{-1} \sum_{i=1}^n I(S_{\boldsymbol{\theta}, i} \geq c)(1 - Y_i)$, $\zeta(c, \boldsymbol{\theta}) = \text{E}[I(S_{\boldsymbol{\theta}} \geq c)(1 - Y)]$, and

$$\widehat{\mathcal{W}}_\zeta(c, \boldsymbol{\theta}) = n^{1/2} \left[\widehat{\zeta}(c, \boldsymbol{\theta}) - \zeta(c, \boldsymbol{\theta}) \right] = \mathbb{G}_n[I(S_{\boldsymbol{\theta}} \geq c)(1 - Y)].$$

Using the same argument as in the previous section,

$$\widehat{\mathcal{W}}_{\text{FPR}}(c) = \mu_0^{-1} \left[\widehat{\mathcal{W}}_\zeta(c, \boldsymbol{\theta}) - \text{FPR}(c; \boldsymbol{\theta}) \widehat{\mathcal{W}}_\zeta(0, \boldsymbol{\theta}) \right] \frac{\zeta(0, \boldsymbol{\theta})}{\widehat{\zeta}(0, \boldsymbol{\theta})},$$

where $\mu_0 = 1 - \mu$. Using an analogous argument as the previous section,

$$\widehat{\mathcal{W}}_\zeta(c, \boldsymbol{\theta}) = n^{-1/2} \sum_{i=1}^n [(1 - Y_i) I(S_{\boldsymbol{\theta}, i} \geq c) - \mu_0 \text{FPR}(c; \boldsymbol{\theta})]$$

converges weakly to a mean zero Gaussian process indexed by $(\boldsymbol{\theta}, c)$, and is stochastic equicontinuous in $(\boldsymbol{\theta}, c)$ so that

$$\begin{aligned}\widehat{\mathcal{W}}_{\text{FPR}}(c) &= \mu_0^{-1} \left[\widehat{\mathcal{W}}_{\zeta}(c, \boldsymbol{\theta}^*) - \text{FPR}(c) \widehat{\mathcal{W}}_{\zeta}(0, \boldsymbol{\theta}^*) \right] + o_p(1) \\ &= \mu_0^{-1} \left\{ n^{-1/2} \sum_{i=1}^n (1 - Y_i) [I(S_i^* \geq c) - \text{FPR}(c)] \right\} + o_p(1) \\ &= n^{-1/2} \sum_{i=1}^n -\mu_0^{-1} \{ (Y_i - \mu) [I(S_i^* \geq c) - \text{FPR}(c)] - \mu_0^{-1} [I(S_i^* \geq c) - \text{FPR}(c)] \} + o_p(1).\end{aligned}$$

Using the fact that $\sup_{u_0 \in [0,1]} |\hat{c}_u - c_{u_0}| = o_p(1)$, it then follows that [Proposition 3.1–3.2, 11]

$$\begin{aligned}\widehat{\mathcal{W}}_{\text{ROC}}(u_0) &= \widehat{\mathcal{W}}_{\text{TPR}}(c_{u_0}) - \text{ROC}(u_0) \widehat{\mathcal{W}}_{\text{FPR}}(c_{u_0}) + o_p(1) \\ &= n^{-1/2} \sum_{i=1}^n [\mathcal{G}_i(S; \boldsymbol{\theta}^*, c_{u_0})(Y_i - \mu) + \Gamma_i(S; \boldsymbol{\theta}^*, c_{u_0})] + o_p(1) \\ &= n^{-1/2} \sum_{i=1}^n IF_{\text{supROC}}(Y_i, S_i; \boldsymbol{\theta}^*, c_{u_0}) + o_p(1)\end{aligned}$$

where $\mathcal{G}_i(S; \boldsymbol{\theta}^*, c_{u_0}) = \left[\mu^{-1} + \mu_0^{-1} \text{ROC}(u_0) \right] I(S_i^* \geq c_{u_0}) - \left[\mu^{-1} \text{ROC}(u_0) + \mu_0^{-1} \text{ROC}(u_0) u_0 \right]$, $\Gamma_i(S; \boldsymbol{\theta}^*, c_{u_0}) = I(S_i^* \geq c_{u_0}) - \text{ROC}(u_0) - \text{ROC}(u_0) [I(S_i^* \geq c_{u_0}) - u_0]$, and $IF_{\text{supROC}}(Y_i, S_i; \boldsymbol{\theta}^*, c_{u_0}) = \mathcal{G}_i(S; \boldsymbol{\theta}^*, c_{u_0})(Y_i - \mu) + \Gamma_i(S; \boldsymbol{\theta}^*, c_{u_0})$. Therefore, $\widehat{\mathcal{W}}_{\text{ROC}}(u_0)$ is asymptotically Gaussian with mean zero and variance $E\{[IF_{\text{supROC}}(Y, S; \boldsymbol{\theta}^*, c_{u_0})]^2\}$.

3.2 Semi-supervised Estimator

We follow the same general steps as in Figure 1 to study the weak convergence of the semi-supervised estimator.

Similar as before, we let g be a measurable function define $\mathbb{P}_N g = N^{-1} \sum_{i=n+1}^{n+N} g(X_i)$, and $\mathbb{G}_N g = N^{1/2}(\mathbb{P}_N g - \mathbb{P}g)$ be the scaled empirical process indexed by g .

Step 1: Weak convergence of $\widetilde{\mathcal{W}}_{\text{TPR}}(c)$

Let $\tilde{\xi}(c, \boldsymbol{\theta}) = N^{-1} \sum_{i=n+1}^{n+N} I(S_{\boldsymbol{\theta},i} \geq c) \widehat{m}(S_{\boldsymbol{\theta},i})$ and $\xi(c, \boldsymbol{\theta}) = \mathbb{E}[I(S_{\boldsymbol{\theta}} \geq c)Y] = \mathbb{E}[I(S_{\boldsymbol{\theta}} \geq c)m(S_{\boldsymbol{\theta}})]$. Following the same steps as in Figure 1, we establish the weak convergence of

$$\begin{aligned} \widetilde{\mathcal{W}}_{\xi}(c, \boldsymbol{\theta}) &= n^{1/2} \left[\tilde{\xi}(c, \boldsymbol{\theta}) - \xi(c, \boldsymbol{\theta}) \right] \\ &= \widetilde{\mathcal{W}}_{\xi,a} + \widetilde{\mathcal{W}}_{\xi,b}, \end{aligned}$$

where $\widetilde{\mathcal{W}}_{\xi,a} = n^{1/2} \mathbb{P}_N \{I(S_{\boldsymbol{\theta}} \geq c) [\widehat{m}(S_{\boldsymbol{\theta}}) - m(S_{\boldsymbol{\theta}})]\}$ and $\widetilde{\mathcal{W}}_{\xi,b} = (n/N)^{1/2} \mathbb{G}_N [I(S_{\boldsymbol{\theta}} \geq c)m(S_{\boldsymbol{\theta}})]$.

For $\widetilde{\mathcal{W}}_{\xi,b}$, we note that $\mathbb{G}_N [I(S_{\boldsymbol{\theta}} \geq c)m(S_{\boldsymbol{\theta}})]$ converges weakly to a Gaussian process by the functional Central Limit Theorem [Theorem 10.6, 12] and therefore

$$\widetilde{\mathcal{W}}_{\xi,b} = (n/N)^{1/2} \mathbb{G}_N [I(S_{\boldsymbol{\theta}} \geq c)m(S_{\boldsymbol{\theta}})] = O_p \left[(n/N)^{1/2} \right] = o_p(1).$$

For $\widetilde{\mathcal{W}}_{\xi,a}$, we write $\widetilde{\mathcal{W}}_{\xi,a} = \widetilde{\mathcal{W}}_{\xi,a_1} + \widetilde{\mathcal{W}}_{\xi,a_2}$, where

$$\begin{aligned} \widetilde{\mathcal{W}}_{\xi,a_1} &= n^{1/2} (\mathbb{P}_N - \mathbb{P}) \{I(S_{\boldsymbol{\theta}} \geq c) [\widehat{m}(S_{\boldsymbol{\theta}}) - m(S_{\boldsymbol{\theta}})]\} \\ \widetilde{\mathcal{W}}_{\xi,a_2} &= n^{1/2} \mathbb{P} \{I(S_{\boldsymbol{\theta}} \geq c) [\widehat{m}(S_{\boldsymbol{\theta}}) - m(S_{\boldsymbol{\theta}})]\}. \end{aligned}$$

We first evaluate $\widetilde{\mathcal{W}}_{\xi,a_1}$ by considering $\epsilon_i = \{I(S_{\boldsymbol{\theta},i} \geq c) [\widehat{m}(S_{\boldsymbol{\theta},i}) - m(S_{\boldsymbol{\theta},i})]\}_{i=n+1, \dots, n+N}$. Note that ϵ_i are independent conditional on the labeled data and bounded by $|\epsilon_i| \leq \sup_{\mathbf{Z}} |\widehat{m}[S(\mathbf{Z}; \boldsymbol{\theta})] - m[S(\mathbf{Z}; \boldsymbol{\theta})]| = o_p(1) \leq M$ almost surely, for some constant $M < \infty$. Applying Hoeffding's inequality conditional on the labeled data, we have for any $t > 0$,

$$P \left(\sum_{i=1}^N [\epsilon_i - \mathbb{E}(\epsilon_i)] \geq N^{1/2} t \right) \leq \exp \left(-\frac{2Nt^2}{NM^2} \right).$$

Hence $\widetilde{\mathcal{W}}_{\xi,a_1} = O_p \left[(n/N)^{1/2} \right] = o_p(1)$.

Next, to evaluate $\widetilde{\mathcal{W}}_{\xi, a_2}$ we further decompose the term as

$$\begin{aligned}
\widetilde{\mathcal{W}}_{\xi, a_2} &= n^{1/2} \int_c^1 [\widehat{m}(s_{\boldsymbol{\theta}}) - m(s_{\boldsymbol{\theta}})] f(s_{\boldsymbol{\theta}}) ds_{\boldsymbol{\theta}} \\
&= n^{1/2} \int_c^1 [\widehat{m}(s_{\boldsymbol{\theta}}) - m(s_{\boldsymbol{\theta}})] \left[f(s_{\boldsymbol{\theta}}) + \widehat{f}(s_{\boldsymbol{\theta}}) - \widehat{f}(s_{\boldsymbol{\theta}}) \right] ds_{\boldsymbol{\theta}} \\
&= n^{1/2} \int_c^1 \sum_{i=1}^n \frac{1}{nh} K_h(S_{\boldsymbol{\theta}, i} - s_{\boldsymbol{\theta}}) [Y_i - m(s_{\boldsymbol{\theta}})] ds_{\boldsymbol{\theta}} + n^{1/2} \int_c^1 [\widehat{m}(s_{\boldsymbol{\theta}}) - m(s_{\boldsymbol{\theta}})] \left[f(s_{\boldsymbol{\theta}}) - \widehat{f}(s_{\boldsymbol{\theta}}) \right] ds_{\boldsymbol{\theta}} \\
&= \widetilde{\mathcal{W}}_{\xi, a_{21}} + \widetilde{\mathcal{W}}_{\xi, a_{22}},
\end{aligned}$$

where $\widehat{f}(s) = \frac{1}{n} \sum_{i=1}^n K_h(S_{\boldsymbol{\theta}, i} - s_{\boldsymbol{\theta}})$.

From Assumption 3, it follows from [Lemma 1 and Theorem B, 13] that

$$\widetilde{\mathcal{W}}_{\xi, a_{22}} \leq n^{1/2} \sup_{s_{\boldsymbol{\theta}} \in [c, 1]} |\widehat{m}(s_{\boldsymbol{\theta}}) - m(s_{\boldsymbol{\theta}})| \sup_{s_{\boldsymbol{\theta}} \in [c, 1]} |f(s_{\boldsymbol{\theta}}) - \widehat{f}(s_{\boldsymbol{\theta}})| = O_p \left[\frac{\log(1/h)}{n^{1/2}h} \right] = o_p(1).$$

For $\widetilde{\mathcal{W}}_{\xi, a_{21}}$, we substitute $u_0 = (s_{\boldsymbol{\theta}} - S_{\boldsymbol{\theta}, i})/h$ and apply Taylor's expansion at $S_{\boldsymbol{\theta}, i}$,

$$\begin{aligned}
\widetilde{\mathcal{W}}_{\xi, a_{21}} &= n^{-1/2} \sum_{i=1}^n \int_{(c-S_{\boldsymbol{\theta}, i})/h}^{(1-S_{\boldsymbol{\theta}, i})/h} K(u_0) [Y_i - m(hu_0 + S_{\boldsymbol{\theta}, i})] du \\
&= n^{-1/2} \sum_{i=1}^n \int_{(c-1)/h}^{(1-c)/h} I(S_{\boldsymbol{\theta}, i} \geq c) K(u_0) [Y_i - m(S_{\boldsymbol{\theta}, i}) - uhm'(S_{\boldsymbol{\theta}, i}) - u_0^2 h^2 m''(S_{\boldsymbol{\theta}, i})/2 + o(h^2)] du \\
&= n^{-1/2} \sum_{i=1}^n I(S_{\boldsymbol{\theta}, i} \geq c) [Y_i - m(S_{\boldsymbol{\theta}, i})] + O_p(n^{1/2}h^2)
\end{aligned}$$

It then follows that

$$\widetilde{\mathcal{W}}_{\xi}(c, \boldsymbol{\theta}) = n^{-1/2} \sum_{i=1}^n I(S_{\boldsymbol{\theta}, i} \geq c) [Y_i - m(S_{\boldsymbol{\theta}, i})] + o_p(1)$$

converges weakly to a mean zero Gaussian process indexed by $(\boldsymbol{\theta}, c)$, by the functional Central Limit Theorem [Theorem 10.6, 12] and is stochastic equicontinuous in $(\boldsymbol{\theta}, c)$.

Thus,

$$\begin{aligned}\widetilde{\mathcal{W}}_{\text{TPR}}(c) &= \mu^{-1} \left[\widetilde{\mathcal{W}}_{\xi}(c, \boldsymbol{\theta}^*) - \text{TPR}(c) \widetilde{\mathcal{W}}_{\xi}(0, \boldsymbol{\theta}^*) \right] + o_p(1) \\ &= n^{-1/2} \sum_{i=1}^n \mu^{-1} \{ [Y_i - m(S_i^*)] [I(S_i^* \geq c) - \text{TPR}(c)] \} + o_p(1).\end{aligned}$$

Step 2: Weak convergence of $\widetilde{\mathcal{W}}_{\text{FPR}}(c)$

Let $\tilde{\zeta}(c, \boldsymbol{\theta}) = N^{-1} \sum_{i=n+1}^{n+N} I(S_{\boldsymbol{\theta},i} \geq c) [1 - \widehat{m}(S_{\boldsymbol{\theta},i})]$, $\zeta(c, \boldsymbol{\theta}) = \text{E} \{ I(S_{\boldsymbol{\theta}} \geq c) [1 - m(S_{\boldsymbol{\theta}})] \}$, and

$$\widetilde{\mathcal{W}}_{\zeta}(c, \boldsymbol{\theta}) = n^{1/2} \left[\tilde{\zeta}(c, \boldsymbol{\theta}) - \zeta(c, \boldsymbol{\theta}) \right].$$

Using the same argument as in the previous section,

$$\widetilde{\mathcal{W}}_{\text{FPR}}(c) = \mu_0^{-1} \left[\widetilde{\mathcal{W}}_{\zeta}(c, \boldsymbol{\theta}) - \text{FPR}(c; \boldsymbol{\theta}) \widetilde{\mathcal{W}}_{\zeta}(0, \boldsymbol{\theta}) \right] \frac{\zeta(0, \boldsymbol{\theta})}{\zeta(0, \boldsymbol{\theta})},$$

where $\mu_0 = 1 - \mu$. Using analogous arguments as the supervised setting,

$$\widetilde{\mathcal{W}}_{\zeta}(c, \boldsymbol{\theta}) = n^{-1/2} \sum_{i=1}^n \{ [m(S_{\boldsymbol{\theta},i}) - Y_i] I(S_{\boldsymbol{\theta},i} \geq c) \}$$

converges weakly to a mean zero Gaussian process index by $(\boldsymbol{\theta}, c)$, and is stochastic equicontinuous in $(\boldsymbol{\theta}, c)$ so that

$$\begin{aligned}\widetilde{\mathcal{W}}_{\text{FPR}}(c) &= \mu_0^{-1} \left[\widetilde{\mathcal{W}}_{\xi}(c, \boldsymbol{\theta}^*) - \text{FPR}(c) \widetilde{\mathcal{W}}_{\xi}(0, \boldsymbol{\theta}^*) \right] + o_p(1) \\ &= n^{-1/2} \sum_{i=1}^n -\mu_0^{-1} \{ [Y_i - m(S_i^*)] [I(S_i^* \geq c) - \text{FPR}(c)] \} + o_p(1).\end{aligned}$$

It then follows that

$$\begin{aligned}
\widetilde{\mathcal{W}}_{\text{ROC}}(u_0) &= \widetilde{\mathcal{W}}_{\text{TPR}}(c_{u_0}) - \text{ROC}(u_0)\widetilde{\mathcal{W}}_{\text{FPR}}(c_{u_0}) + o_p(1) \\
&= n^{-1/2} \sum_{i=1}^n \mathcal{G}_i(S; \boldsymbol{\theta}^*, c_{u_0}) [Y_i - m(S_i^*)] + o_p(1) \\
&= n^{-1/2} \sum_{i=1}^n IF_{ss\text{ROC}}(Y_i; \boldsymbol{\theta}^*, c_{u_0}) + o_p(1)
\end{aligned}$$

where $\mathcal{G}_i(S; \boldsymbol{\theta}^*, c_{u_0}) = \left[\mu^{-1} + \mu_0^{-1} \text{ROC}(u_0) \right] I(S_i^* \geq c_{u_0}) - \left[\mu^{-1} \text{ROC}(u_0) + \mu_0^{-1} \text{ROC}(u_0) u_0 \right]$, and $IF_{ss\text{ROC}}(Y_i, S_i; \boldsymbol{\theta}^*, c_{u_0}) = \mathcal{G}_i(S; \boldsymbol{\theta}^*, c_{u_0}) [Y_i - m(S_i^*)]$. Therefore, $\widetilde{\mathcal{W}}_{\text{ROC}}(u_0)$ is asymptotically Gaussian with mean zero and variance $E\{[IF_{ss\text{ROC}}(Y, S; \boldsymbol{\theta}^*, c_{u_0})]^2\}$.

4 Description of the PheNorm Algorithm

We briefly outline the PheNorm algorithm proposed by [4], which consists of three key steps. We do not use the random corruption denoising step as it showed limited improvement in the original paper.

Step I: Raw Feature Extraction. The input data for PheNorm is patient-level data on $(x_{ICD}, x_{NLP}, x_{ICDNLP}, x_{HU})$. The *silver-standard labels* are x_{ICD} , x_{NLP} , and $x_{ICDNLP} = x_{ICD} + x_{NLP}$. x_{ICD} and x_{NLP} are the counts of phenotype-specific ICD codes and free-text positive mentions of target phenotype in a patient’s record. x_{ICDNLP} is a derived feature that can be more predictive of the underlying phenotype than x_{ICD} or x_{NLP} alone. x_{HU} is a feature measuring *healthcare utilization* such as the count of the total number of notes in a patient’s record or the number of encounters in the billing system.

Step II: Normal Mixture Normalization. The silver-standard labels are normalized against x_{HU} to account for the fact that patients with higher healthcare utilization tend to have more ICD codes and free-text positive mentions of target phenotype, irrespective of their true disease status. The key idea of PheNorm is that the normalized silver standard labels approximately follow a normal mixture model.

Specifically, let

$$z = \log(1 + x_s) - \alpha \log(1 + x_{HU})$$

be a normalized silver-standard label for some $\alpha \in (0, 1)$ and $s \in (ICD, NLP, ICDNLP)$. PheNorms assumes

$$z \sim \mu N(\tau_1, \sigma^2) + (1 - \mu)N(\tau_0, \sigma^2)$$

where $\mu = P(Y = 1)$, τ_1 and τ_0 are the means corresponding to the phenotype case and control groups, respectively, and σ^2 is a common variance parameter. The PheNorm

algorithm finds estimates for $(\alpha, \mu, \tau_0, \tau_1, \sigma)$ through the expectation-maximization (EM) algorithm. The optimal value of the normalization coefficient, α , minimizes the distribution divergence between the empirical distribution of the observed z and the normal mixture approximation. For a given α , the EM algorithm is used to find the maximum likelihood estimates of $(\mu, \tau_0, \tau_1, \sigma)$, and the distributional divergence is calculated using the parameter estimates.

Step III: Majority Voting. The normal mixture approximation in Step II is utilized for all three of the silver-standard labels. With the normal mixture parameter estimates, the posterior probability of the phenotype is calculated based on each silver standard label. The final PheNorm score is the average of the three posterior probabilities.

5 Simulation Study

| Metric | n | Method | ESE | ASE | Coverage Probability | |
|-----------|-----|--------|-------|-------|----------------------|-------------|
| | | | | | Standard Wald | Logit-based |
| AUC | 100 | supROC | 5.70 | 5.76 | 94.10 | 96.05 |
| | | ssROC | 5.71 | 5.50 | 92.60 | 94.80 |
| | 200 | supROC | 3.96 | 4.04 | 95.40 | 96.15 |
| | | ssROC | 3.95 | 3.92 | 94.25 | 95.05 |
| Threshold | 100 | supROC | 4.43 | 4.68 | 92.90 | 93.65 |
| | | ssROC | 3.23 | 3.14 | 91.50 | 91.25 |
| | 200 | supROC | 3.21 | 3.31 | 94.15 | 94.05 |
| | | ssROC | 2.28 | 2.28 | 93.40 | 93.15 |
| TPR | 100 | supROC | 10.60 | 11.14 | 94.20 | 97.55 |
| | | ssROC | 10.16 | 9.96 | 91.55 | 95.60 |
| | 200 | supROC | 7.59 | 7.92 | 95.40 | 97.00 |
| | | ssROC | 7.26 | 7.21 | 92.85 | 95.05 |
| PPV | 100 | supROC | 10.30 | 10.80 | 94.05 | 96.90 |
| | | ssROC | 9.82 | 9.61 | 92.40 | 94.75 |
| | 200 | supROC | 7.02 | 7.44 | 95.20 | 96.70 |
| | | ssROC | 6.72 | 6.76 | 93.85 | 94.50 |
| NPV | 100 | supROC | 4.94 | 5.05 | 94.40 | 96.60 |
| | | ssROC | 4.77 | 4.64 | 92.75 | 95.40 |
| | 200 | supROC | 3.52 | 3.58 | 95.00 | 95.85 |
| | | ssROC | 3.43 | 3.35 | 93.65 | 95.20 |

Table 1: **Coverage Probability for simulation setting 1 at a FPR of 10%.** Coverage Probability (CP) of the 95% confidence intervals for the ROC parameters with labeled data sizes $n = 100$ and 200 for simulation setting 1 (PA with low accuracy). The size of the unlabeled data was $N = 10,000$. ESE: Empirical Standard Error; ASE: Asymptotic Standard Error.

| Metric | n | Method | ESE | ASE | Coverage Probability | |
|-----------|-----|--------|------|------|----------------------|-------------|
| | | | | | Standard Wald | Logit-based |
| AUC | 100 | supROC | 1.69 | 1.70 | 90.55 | 98.40 |
| | | ssROC | 1.49 | 1.34 | 88.25 | 93.20 |
| | 200 | supROC | 1.19 | 1.18 | 92.60 | 96.15 |
| | | ssROC | 1.05 | 0.99 | 91.75 | 93.65 |
| Threshold | 100 | supROC | 3.94 | 4.18 | 93.55 | 94.05 |
| | | ssROC | 2.99 | 2.86 | 91.85 | 92.20 |
| | 200 | supROC | 2.82 | 3.00 | 94.45 | 94.30 |
| | | ssROC | 2.10 | 2.10 | 93.60 | 93.80 |
| TPR | 100 | supROC | 7.83 | 8.26 | 91.45 | 94.89 |
| | | ssROC | 6.50 | 6.29 | 89.50 | 95.65 |
| | 200 | supROC | 5.59 | 5.88 | 93.30 | 98.35 |
| | | ssROC | 4.60 | 4.66 | 92.60 | 96.85 |
| PPV | 100 | supROC | 4.05 | 4.35 | 95.90 | 96.45 |
| | | ssROC | 2.66 | 2.66 | 92.15 | 92.65 |
| | 200 | supROC | 2.77 | 2.93 | 96.15 | 96.20 |
| | | ssROC | 1.83 | 1.86 | 94.25 | 94.20 |
| NPV | 100 | supROC | 3.46 | 3.63 | 90.25 | 94.84 |
| | | ssROC | 2.74 | 2.65 | 89.75 | 95.50 |
| | 200 | supROC | 2.50 | 2.60 | 93.35 | 97.95 |
| | | ssROC | 1.98 | 1.98 | 92.55 | 97.05 |

Table 2: **Coverage Probability for simulation setting 2 at a FPR of 10%.** Coverage Probability (CP) of the 95% confidence intervals for the ROC parameters with labeled data sizes $n = 100$ and 200 for simulation setting 2 (PA with high accuracy). The size of the unlabeled data was $N = 10,000$. ESE: Empirical Standard Error; ASE: Asymptotic Standard Error.

6 Analysis of 6 PAs from MGB

6.1 Relative Efficiency



Figure 2: **Relative efficiency at a FPR of 10%.** The relative efficiency (RE) of supROC versus ssROC for the ROC parameters for the 6 MGB phenotypes. RE is defined as the ratio of the variance of supROC to that of ssROC.

6.2 Perturbation Resampling

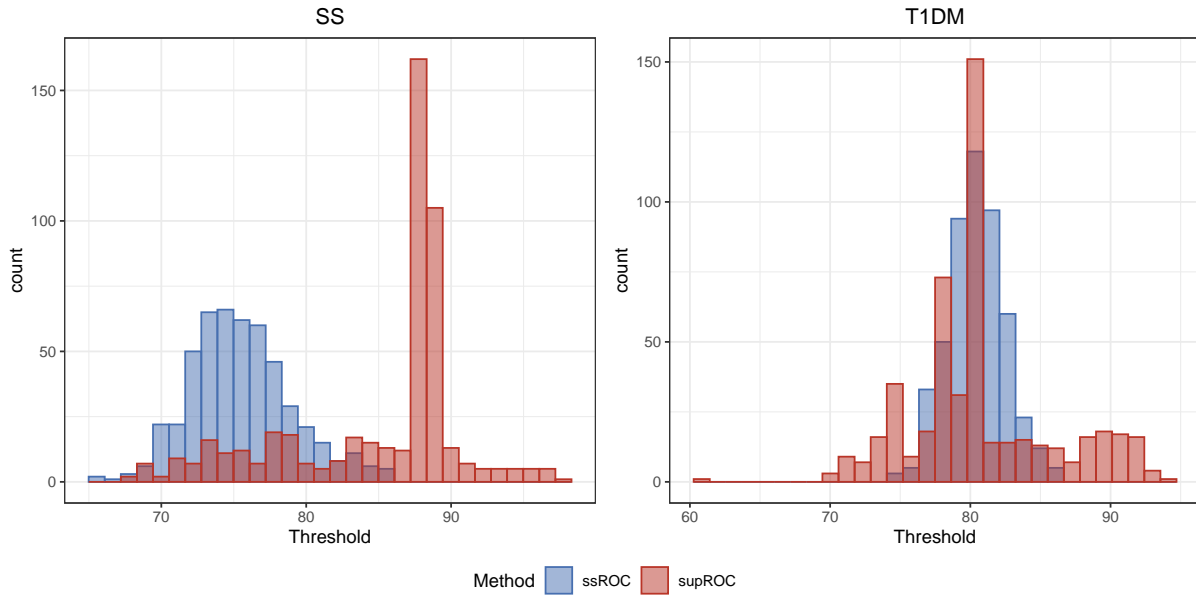


Figure 3: **Empirical Distribution of the Perturbed Threshold at a FPR of 10%.** Distribution of the classification threshold (Threshold) estimates from 500 replicates of the perturbation resampling procedure for Systemic sclerosis (SS) and Type 1 Diabetes (T1DM).

References

1. Jin, Z., Ying, Z. & Wei, L. A Simple Resampling Method by Perturbing the Minimax. *Biometrika* **88**, 381–390 (June 2001).
2. Gronsbell, J. L. & Cai, T. Semi-supervised approaches to efficient evaluation of model prediction performance. *Journal of the Royal Statistical Society: Series B (Statistical Methodology)* **80**, 579–594 (2018).
3. Agresti, A. *Categorical data analysis* (John Wiley & Sons, 2012).
4. Yu, S., Ma, Y., Gronsbell, J., *et al.* Enabling phenotypic big data with PheNorm. *Journal of the American Medical Informatics Association* **25**, 54–60 (2018).
5. Gronsbell, J., Minnier, J., Yu, S., *et al.* Automated feature selection of predictors in electronic medical records data. *Biometrics* **75**, 268–277 (2019).
6. Agarwal, V., Podchiyska, T., Banda, J. M., *et al.* Learning statistical models of phenotypes using noisy labeled training data. *Journal of the American Medical Informatics Association* **23**, 1166–1173 (2016).
7. Banda, J. M., Halpern, Y., Sontag, D., *et al.* Electronic phenotyping with APHRODITE and the Observational Health Sciences and Informatics (OHDSI) data network. *AMIA Summits on Translational Science Proceedings* **2017**, 48–57 (July 2017).
8. Van der Vaart, A. W. *Asymptotic statistics* (Cambridge University Press, 2000).
9. Newey, W. K. & McFadden, D. in *Handbook of Econometrics* 2111–2245 (Elsevier, Jan. 1994).
10. Van der Vaart, A. W. *Asymptotic Statistics* (Cambridge University Press, Cambridge, UK ; New York, NY, USA, 1998).
11. Bogoya, J. M., Böttcher, A. & Maximenko, E. A. From Convergence in Distribution to Uniform Convergence. *Boletín de la Sociedad Matemática Mexicana* **22**, 695–710 (Oct. 2016).

12. Pollard, D. *Empirical processes: theory and applications* in *NSF-CBMS regional conference series in probability and statistics* (1990), i–86.
13. Mack, Y. P. & Silverman, B. W. Weak and Strong Uniform Consistency of Kernel Regression Estimates. *Zeitschrift für Wahrscheinlichkeitstheorie und Verwandte Gebiete* **61**, 405–415 (Sept. 1982).